Mycobacterium marinum produces distinct mycobactin and carboxymycobactin siderophores to promote growth in broth and phagocytes

Paulina Knobloch, Hendrik Koliwer-brandl, Fabian M Arnold, Nabil Hanna, Imre Gonda, Sophia Adenau, Nicolas Personnic, Caroline Barisch, Markus A Seeger, Thierry Soldati, et al.

Received: 26 July 2019 | Accepted: 22 December 2019

DOI: 10.1111/cmi.13163

RESEARCH ARTICLE

WILEY

Mycobacterium marinum produces distinct mycobactin and carboxymycobactin siderophores to promote growth in broth and phagocytes

Paulina Knobloch[1] | Hendrik Koliwer-Brandl[1] | Fabian M. Arnold[1] | Nabil Hanna[2] | Imre Gonda[1] | Sophia Adenau[1] | Nicolas Personnic[1] | Caroline Barisch[2] | Markus A. Seeger[1] | Thierry Soldati[2] | Hubert Hilbi[1]

[1]Institute of Medical Microbiology, University of Zürich, Zürich, Switzerland

[2]Department of Biochemistry, Faculty of Sciences, University of Geneva, Geneva, Switzerland

Correspondence
Hubert Hilbi, Institute of Medical Microbiology, University of Zürich, Zürich, Switzerland.
Email: hilbi@imm.uzh.ch

Present address
Division of Molecular Infection Biology, Department of Biology/ Chemistry, University of Osnabrück, 49076 Osnabrück, Germany.

Funding information
H2020 European Research Council, Grant/Award Number: 772190; Novartis Foundation for Medical-Biological Research; Schweizerischer Nationalfonds zur Förderung der Wissenschaftlichen Forschung, Grant/Award Numbers: 31003A_153200, 31003A_175557, PP00P3_144823, PZ00P3_161492; SystemsX, Grant/Award Number: HostPathX; SNF Ambizione program, Grant/Award Number: PZ00P3_161492; Foundation for Medical-Biological Research; European Research Council, Grant/Award Number: 772190; SNF Professorship, Grant/Award Number: PP00P3_144823; SystemsX.ch project HostPathX; Swiss National Science Foundation, Grant/Award Numbers: 31003A_175557, 31003A_153200

Abstract

Mycobacterium marinum is a model organism for pathogenic *Mycobacterium* species, including *Mycobacterium tuberculosis*, the causative agent of tuberculosis. These pathogens enter phagocytes and replicate within the *Mycobacterium*-containing vacuole, possibly followed by vacuole exit and growth in the host cell cytosol. Mycobacteria release siderophores called mycobactins to scavenge iron, an essential yet poorly soluble and available micronutrient. To investigate the role of *M. marinum* mycobactins, we purified by organic solvent extraction and identified by mass spectrometry the lipid-bound mycobactin (MBT) and the water-soluble variant carboxymycobactin (cMBT). Moreover, we generated by specialised phage transduction a defined *M. marinum* Δ*mbtB* deletion mutant predicted to be defective for mycobactin production. The *M. marinum* Δ*mbtB* mutant strain showed a severe growth defect in broth and phagocytes, which was partially complemented by supplying the *mbtB* gene on a plasmid. Furthermore, purified Fe-MBT or Fe-cMBT improved the growth of wild type as well as Δ*mbtB* mutant bacteria on minimal plates, but only Fe-cMBT promoted the growth of wild-type *M. marinum* during phagocyte infection. Finally, the intracellular growth of *M. marinum* Δ*mbtB* in *Acanthamoeba castellanii* amoebae was restored by coinfection with wild-type bacteria. Our study identifies and characterises the *M. marinum* MBT and cMBT siderophores and reveals the requirement of mycobactins for extra- and intracellular growth of the pathogen.

KEYWORDS

ABC transporter, *Acanthamoeba*, amoeba, bacterial pathogenesis, carboxymycobactin, *Dictyostelium*, exochelin, iron acquisition, macrophage, mycobactin, pathogen vacuole, siderophore, tuberculosis

1 | INTRODUCTION

Mycobacterium marinum is a human pathogen of moderate concern (Aubry, Mougari, Reibel, & Cambau, 2017) and a close relative of *Mycobacterium tuberculosis*, the causative agent of tuberculosis (TB).

Abbreviations: ABC transporter, ATP-binding cassette transporter; cMBT, carboxymycobactin; MBT, mycobactin; MCV, *Mycobacterium*-containing vacuole; MS, mass spectrometry; T7SS, type VII secretion system.

TB is the worldwide prevalent cause of death from a single pathogen, resulting in 1.6 million people killed in 2017 alone. In 2017, about 10 million people developed this disease, 1.7 billion individuals were believed to be latently infected, with drug resistance becoming an ever-increasing concern (World Health Organization, 2019).

M. marinum is widely used as a versatile *M. tuberculosis* infection model (Arafah et al., 2013; Bouz & Al Hasawi, 2018; Cardenal-Munoz, Barisch, Lefrancois, Lopez-Jimenez, & Soldati, 2017; Hagedorn, Rohde, Russell, & Soldati, 2009; Hagedorn & Soldati, 2007; Lienard & Carlsson, 2017; Prouty, Correa, Barker, Jagadeeswaran, & Klose, 2003; Shiloh & Champion, 2010; Tükenmez et al., 2019). *M. marinum* can be handled at biosafety Level 2 and is appreciated for its relatively rapid growth (doubling time of 4–10 hr vs. >20 hr for *M. tuberculosis*; Clark & Shepard, 1963), the *M. tuberculosis*-like behaviour during intracellular infection, such as replication within a distinct *Mycobacterium*-containing vacuole (MCV; Barker, George, Falkow, & Small, 1997; Pozos & Ramakrishnan, 2004; Smith et al., 2008; Tobin & Ramakrishnan, 2008; López-Jiménez et al., 2018; Koliwer-Brandl et al., 2019), as well as its wide spectrum of host cells including macrophages (Barker et al., 1997; Bouley, Ghori, Mercer, Falkow, & Ramakrishnan, 2001; Koliwer-Brandl et al., 2019; Ramakrishnan, Federspiel, & Falkow, 2000) and the amoeba *Dictyostelium discoideum* (Cardenal-Munoz et al., 2017; Hagedorn et al., 2009; Koliwer-Brandl et al., 2019; Solomon, Leung, & Isberg, 2003) or *Acanthamoeba castellanii* (Harrison et al., 2013; Kicka et al., 2014).

Mycobacteria require the micronutrient iron for extra- and intracellular growth, which they acquire through the production of low molecular weight Fe^{3+} chelators termed siderophores (Ratledge & Dover, 2000). Pathogenic mycobacteria, such as *M. tuberculosis*, produce two siderophore variants, which are produced by nonribosomal peptide synthetases and polyketide synthases: the hydrophobic mycobactin (MBT; Snow, 1965) and the more water-soluble carboxymycobactin (cMBT; Gobin et al., 1995), together also referred to as mycobactins (Chao, Sieminski, Owens, & Goulding, 2019; Sritharan, 2016; Wilson, Bogdan, Miyazawa, Hashimoto, & Tsuji, 2016). Environmental, non-pathogenic mycobacteria, such as *Mycobacterium smegmatis*, additionally produce a distinct class of siderophores called exochelins (Horwitz & Horwitz, 2014; Sharman, Williams, Ewing, & Ratledge, 1995).

The mycobactins belong to the mixed type iron scavengers, comprising two hydroxamate and an oxazoline moiety, which together form a tight complex with the ferric iron ion. MBT and cMBT from different mycobacterial species share a similar core structure that comprises derivatives of five amino acids and a salicylate-derived oxazoline ring, which bind ferric iron in a hexadentate manner. Modifications of the core structure differ among mycobacterial species by their alkylation pattern, most characteristic is a long aliphatic chain (MBT) or—located at the same position—a much shorter terminally carboxylated acyl chain (cMBT;Chao et al., 2019; Sritharan, 2016). *M. marinum* MBT shares the general scaffold of the mycobactin core with other mycobacterial mycobactins; however, the long aliphatic chain localises differently and is attached to the backbone rather than the peripheral hydroxamate. Moreover, *M. marinum* produces two forms of MBT: the dominant M form and the much less abundant N form, with a $-H$ or $-CH_3$ moiety, respectively, at the peripheral hydroxamate (Snow & White, 1969; White & Snow, 1968). *M. marinum* cMBT has not been characterised.

The export and import of (Fe-)MBT and (Fe-)cMBT across the mycobacterial membranes and waxy cell wall are complex and not well understood (Chao et al., 2019; Sritharan, 2016). The water-soluble cMBT is released into the environment, where it retrieves Fe^{3+} ions in soluble form or, in case of pathogenic mycobacteria, from iron-containing host proteins such as transferrin or lactoferrin (Sritharan, 2016; Chao et al., 2019). The lipophilic MBT localises to mycobacterial membranes and the cell wall and remains membrane/cell wall-bound (Ratledge, Patel, & Mundy, 1982; Touchette & Seeliger, 2017), but can also be released in membrane vesicles (MVs) and thus might bind Fe^{3+} beyond the immediate vicinity of the bacteria (Gupta & Rodriguez, 2018; Prados-Rosales et al., 2014).

The import of iron-loaded cMBT across the inner membrane involves the heterodimeric ABC transporter IrtAB, the production of which is negatively regulated by the iron-dependent repressor, IdeR (Chao et al., 2019; Rodriguez & Smith, 2006; Sritharan, 2016). IrtA contains a highly conserved, N-terminal siderophore-interacting domain, which is likely involved in the reduction of mycobactin-bound ferric iron at the cytoplasmc side of the inner membrane and the consequent release of ferrous iron (Ryndak, Wang, Smith, & Rodriguez, 2010). Compared with MBT, cMBT has a more amphipathic character, and Fe-cMBT might traverse the membrane—at least to some extent—without support from transporters (Horwitz & Horwitz, 2014).

In *M. tuberculosis*, two gene clusters encode the enzymes involved in mycobactin synthesis: *mbt-1* (*mbtA* to *mbtJ*), catalysing the synthesis of the mycobactin core structure, and *mbt-2* (genes *mbtK* to *mbtN*), assembling the hydrophobic side chain (Chao et al., 2019; Sritharan, 2016). In several studies, the *mbt* genes have been found to be required for mycobactin biosynthesis (McMahon, Rush, & Thomas, 2012; Quadri, Sello, Keating, Weinreb, & Walsh, 1998) and *M. tuberculosis* virulence (De Voss et al., 2000; Madigan et al., 2015; Reddy et al., 2013; Tufariello et al., 2016). The *mbtA-J* and *irtAB* genes are induced in *M. tuberculosis*-infected macrophages after host cell activation (Rohde, Abramovitch, & Russell, 2007; Rohde, Veiga, Caldwell, Balazsi, & Russell, 2012; Schnappinger et al., 2003; Tailleux et al., 2008). In *M. smegmatis* and *M. marinum*, the genomic organisation of the *mbt* genes shares similarities with *M. tuberculosis*, yet their function has not been further characterised (Figure S1, Table S1–S3).

Here, we set out to biochemically and genetically characterise the role of mycobactins for growth of *M. marinum* in broth and in phagocytes. To this end, we purified and identified *M. marinum* MBT as well as cMBT. Moreover, we found that *M. marinum* Δ*mbtB* mutant strains show growth defects in broth and phagocytes, which can be genetically complemented and reversed by purified mycobactins.

2 | RESULTS

2.1 | Purification and identification of *M. marinum* mycobactins

Pathogenic *Mycobacterium* species usually produce two kinds of mycobactin siderophores: the lipid-soluble MBT and the water-soluble cMBT (Ramakrishnan et al., 2000), but for *M. marinum*, only MBT has

been identified and characterised thus far (Snow & White, 1969; White & Snow, 1968). To assess whether *M. marinum* produces MBT as well as cMBT, we set out to biochemically purify the compounds. Upon growth in a liquid minimal medium established to purify *M. smegmatis* MBT (see Materials and Methods), the *M. marinum* M strain produced only little amounts of the siderophore, as indicated by the absence of the typical red-brown colour of ferrimycobactin (Fe-MBT) upon ethanol/chloroform extraction and Fe^{3+} saturation. However, upon growth of the strain on the corresponding agarose minimal medium plates, the iron-saturated extract turned red, indicating that MBT was produced and extracted in high amounts (Figure S2). Varying the concentration of Fe^{2+} in the solidified minimal medium affected the MBT production, with maximum amounts being produced at a concentration of 0.32 μg/ml Fe^{2+} (5.7 μM $FeSO_4$; Figure S2a). Moreover, the yield of MBT was much higher when bacteria were evenly spread on agar plates, thereby disintegrating bacterial clumps. Extracted *M. marinum* Fe-MBT yielded a single peak after size-exclusion chromatography (SEC; Figure S2b) and showed the characteristic absorbance maximum at 450 nm (Figure S2c), like *M. smegmatis* Fe-MBT after SEC (Figure S2d).

To determine the structure of *M. marinum* Fe-MBT, we used matrix-assisted laser desorption/ionisation (MALDI)–time of flight (TOF) tandem mass spectrometry (MS/MS). In this approach, dominant peaks at m/z of 830, 844, 858, 883, 897, and 911 (Figure 1a) were subjected to MS/MS analysis (Figure S3). The fragmentation pattern of these peaks is in agreement with the structure of *M. marinum* MBT shown in Figure 1b and the Fe^{3+}-bound form (Figure 1c). *M. marinum* MBT carries different residues attached to the peripheral hydroxamate group (Figure S3a; R_1) or the central ester group of the chelator (Figure S3a; R_2). The m/z values are in agreement with R_1 comprising a hydrogen atom (M form) or a methyl group (N form), and the length of the long acyl chain R_2 varies from C_{15} to C_{17} (M form) or possibly from C_{14} to C_{16} (N form; Figure S3b). The tandem MS analysis indicated that the M form is predominant. The m/z values 830, 844, and 858 correspond to the apo form of MBT (Figure S3c–f), whereas the m/z values 883, 897, and 911 correspond to Fe-MBT (Figure S3g–j). Thus, all dominant m/z peaks in the region of interest are accounted for. Intriguingly, in MBT of *M. marinum*, the long acyl side chain (R_2) is attached adjacent to the central ester group, whereas in MBT of *M. tuberculosis*, *M. smegmatis*, and other mycobacterial species, the long acyl chain is attached to the peripheral hydroxamate moiety (Chao et al., 2019; Sritharan, 2016).

In contrast to MBT, *M. marinum* cMBT was produced in the liquid minimal medium used to produce *M. smegmatis* cMBT but lacking any supplemental iron (see Materials and Methods). *M. marinum* Fe-cMBT purified by ethyl acetate extraction yielded a single peak after SEC (Figure S2e) and showed the characteristic absorbance maximum at 450 nm (Figure S2f), like *M. smegmatis* Fe-cMBT after SEC (Figure S2g). Addition of $FeCl_3$ (≥0.04 μg/ml) to the liquid minimal medium dramatically decreased the production of *M. marinum* cMBT, as indicated by the intensity decrease of the red-brown colour of Fe-MBT upon extraction and Fe^{3+} saturation.

To determine the structure of *M. marinum* cMBT, we used electrospray ionisation (ESI)-qTOF MS/MS. In this approach, dominant peaks at m/z of 773, 787, 801, 815, 829, 843, and 857 (Figure 1d) were subjected to MS/MS analysis (Figure S4). The fragmentation pattern of representative peaks is in agreement with the structure of *M. marinum* cMBT shown in Figure 1e and its Fe^{3+}-bound form (Figure 1f). Like MBT, *M. marinum* cMBT carries different residues attached to the peripheral hydroxamate group (Figure S4a; R_1) or the central ester group of the chelator (Figure S4a; R_2). The m/z values are in agreement with R_1 comprising a hydrogen atom (M form) or a methyl group (N form), and the length of the carboxylated acyl chain R_2 of the representative peaks varies from C_7 to C_9 (M form) or from C_6 to C_8 (N form; Figure S4b). The tandem MS analysis indicated that the M form is predominant. The m/z values 773, 787, 801, 815, 829, 843, and 857 differ by an m/z of 14 (-CH_2-) and correspond to different Fe-cMBT species (Figure S4c–f). Thus, all dominant m/z peaks in the region of interest are accounted for. Like for MBT, in cMBT of *M. marinum*, the acyl side chain with a terminal carboxyl group (R_2) is attached adjacent to the central ester group, whereas in cMBT of *M. tuberculosis*, *M. smegmatis*, and other mycobacterial species, the corresponding chain is attached to the peripheral hydroxamate moiety (Chao et al., 2019; Sritharan, 2016). In summary, *M. marinum* produces distinct MBT and cMBT siderophores, where the long acyl chain or the shorter, terminally carboxylated acyl chain is attached adjacent to the central ester group rather than to the peripheral hydroxamate.

2.2 | Genomic organisation and transcriptome analysis of *M. marinum* mycobactin genes

Having established the production, purification, and identification of *M. marinum* Fe-MBT and Fe-cMBT, we next addressed the genetics of mycobactin biosynthesis. In *M. marinum*, the *mbt* genes putatively involved in mycobactin biosynthesis are mainly organised in one cluster, which due to its similarity with the composition and organisation of the *M. tuberculosis mbt1* locus, we term *M. marinum mbt1* locus (Figure S1). Notably, whereas *mbtB* is organised as the first gene of a putative operon (the first *mbt* gene after an IdeR box) in *M. tuberculosis* and *M. smegmatis*, *mbtB* is located at the end of the orthologous operon in *M. marinum* (Figure S1). Several other *mbt* homologues are dispersed throughout the *M. marinum* genome. In particular, these are orphan homologues of *mbtH* and *mbtK*, the latter localising to the *mbt2* locus in *M. tuberculosis*.

In order to get an understanding of the regulation of the *mbt* genes, we investigated the transcriptomic profile of *M. marinum* grown in 7H9 medium and during infection of *D. discoideum* using RNAseq. The ratio of normalised counts indicated that all *M. marinum mbt1* locus genes, except *mbtH_1* and *mbtJ*, showed a higher level of expression compared with the average read counts of the total genes at each specific condition (Figure 2a, Table S4). The *mbtB* gene showed one of the highest ratio differences, alongside *mbtE* and *mbtF*, with almost fourfold more read counts compared with the average

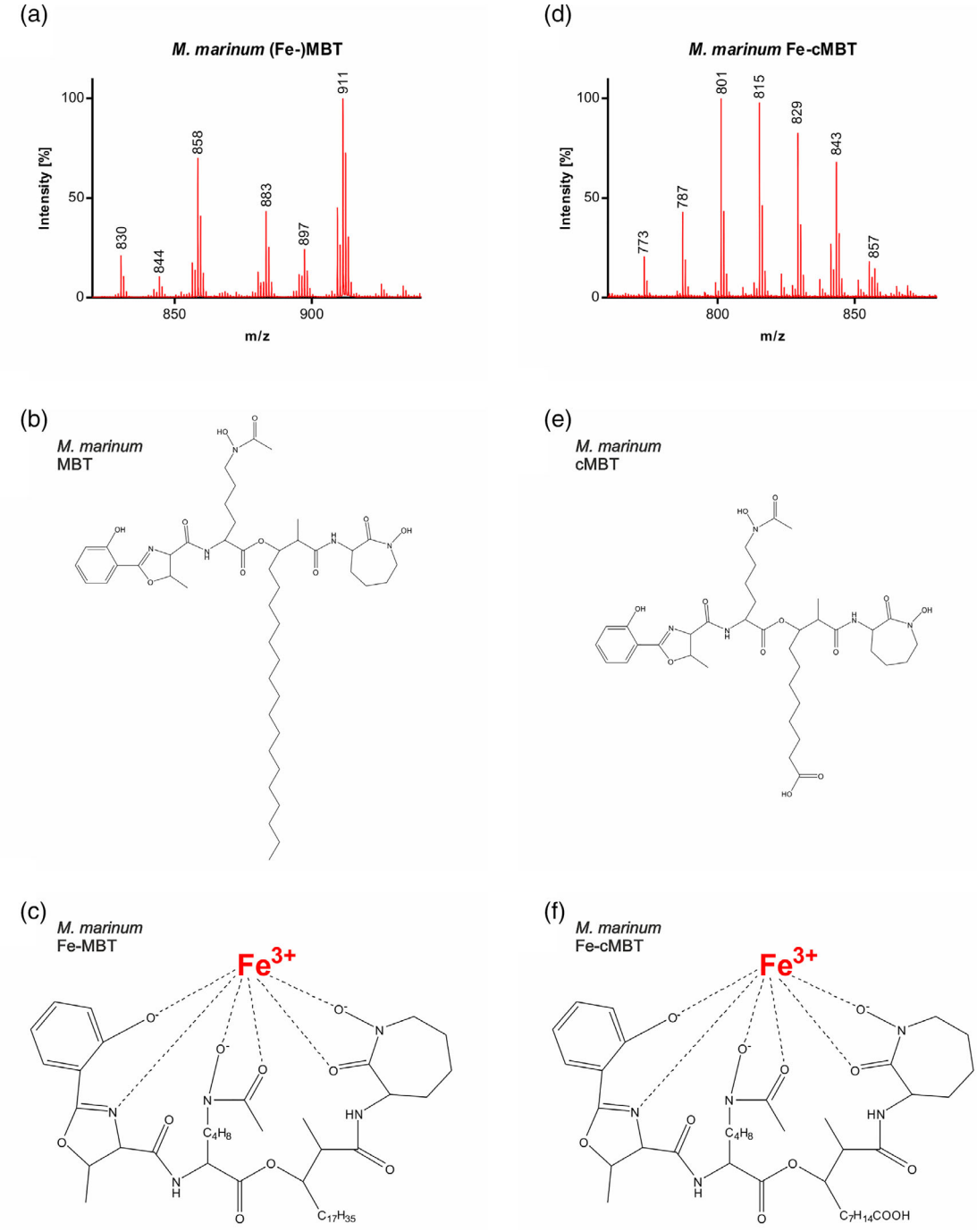

FIGURE 1 Identification of *Mycobacterium marinum* mycobactins. The mycobactins MBT and cMBT were purified by ethanol/chloroform or ethyl acetate extraction from *M. marinum* grown on solidified or in liquid minimal medium, respectively, and saturated with $FeCl_3$, yielding Fe-MBT and Fe-cMBT. (a) MALDI-TOF m/z signals (without and with Fe^{3+}; Δm/z 53) of ethanol/chloroform-extracted *M. marinum* MBT/Fe-MBT. Structural formula of the main *M. marinum* MBT compound (b) without iron, and (c) with Fe^{3+} chelated by the oxazoline and the two hydroxamate moieties of MBT. (d) ESI-qTOF m/z signals (with Fe^{3+}) of ethyl acetate-extracted *M. marinum* Fe-cMBT. Structural formula of the main *M. marinum* cMBT compound (b) without iron and (c) with Fe^{3+} chelated by the oxazoline and the two hydroxamate moieties of cMBT. cMBT, carboxymycobactin; Fe-cMBT, ferrimycobactin; MBT, mycobactin

reads in both in vitro and in vivo (intracellular) conditions. On the other hand, the orphan *mbt* genes and the *mbt2* locus (*mbtK*) showed a lower normalised read count (Figure 2b, Table S4).

In parallel, we investigated the temporal regulatory patterns of *mbt* genes during infection of amoebae compared with growth in broth. The differential expression showed that *mbtJ*, *mbtH_1*, and *mbtF* are up-

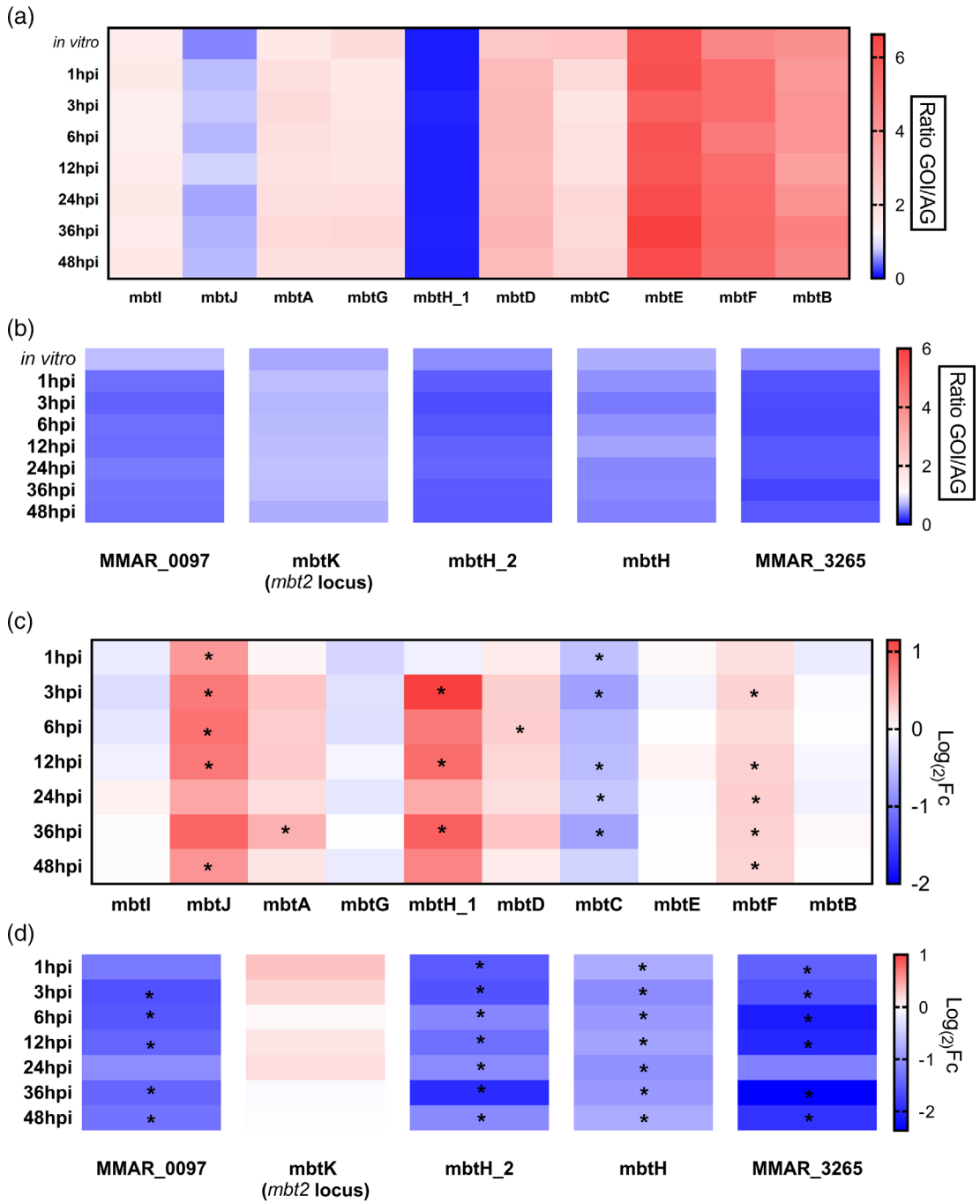

FIGURE 2 Transcriptome analysis of *Mycobacterium marinum* mycobactin genes. Heat maps representing the transcriptional data shown in Table S4. *M. marinum* wild-type bacteria were collected at late exponential phase for the in vitro condition, or *D. discoideum* amoebae were infected with *M. marinum* wild-type, and samples were collected at the indicated time postinfection (hours postinfection, hpi). (a and b) Colours indicate the strength of expression of the different *mbt* genes (GOI) normalised read counts compared with the average of read counts of all the genes (AG) under in vitro conditions or in infected cells: blue (negative ratio), white (no expression difference), or dark red (positive ratio). (c and d) The time points with statistically significant differential expression ($p < .1$) are marked with an asterisk. Colours indicate the expression levels of *mbt* genes (in logFC) of *M. marinum* during infection at the indicated time points compared with the in vitro control: blue (down-regulated during infection), white (no expression difference), or dark red (up-regulated)

regulated at various infection time points, whereas *mbtK* showed a slight up-regulation, and the orphan *mbt* genes were down-regulated during infection (Figure 2c, d; Table S4). Taken together, the RNAseq data show that the *mtb1* locus genes were up-regulated in broth as well as in amoeba host cells, suggesting that under extra- and intracellular conditions, mycobactin siderophores are required for growth.

2.3 | Chromosomal deletion of *M. marinum mbtB* and *irtAB* by phage transduction

To assess the role of mycobactin biosynthesis and transport for *M. marinum* growth in broth and host cells, we constructed defined deletion mutant strains lacking the gene encoding the putative phenyloxazoline synthase MtbB (*mbtB*, MMAR_3689), required for an initial step in siderophore synthesis, or lacking *mbtB* and in addition genes encoding the iron-regulated ABC transporter IrtAB (*irtA*, MMAR_4037; *irtB*, MMAR_4036). Using phage transduction (Koliwer-Brandl et al., 2019), we obtained a *M. marinum* strain, wherein the *mbtB* gene was replaced by a hygromycin resistance cassette and the *sacB* gene. In a second transduction step, the unmarked single deletion mutant strain Δ*mbtB* was generated by removing the *res*-site-flanked resistance cassette with the resolvase-producing phage phAE7.1 and subsequent counter selection for the absence of *sacB*. The Δ*mbtB* strain was used to generate by phage transduction the double knockout strain Δ*mbtB*-Δ*irtAB*$_{Hyg}$, as it was not possible to generate the Δ*irtAB* strain from *M. marinum* wild-type. All gene deletions were verified by polymerase chain reaction (PCR) and sequencing (Figure S5).

2.4 | *M. marinum* Δ*mbtB* and Δ*mbtB*-Δ*irtAB*$_{Hyg}$ are impaired for growth in broth

To test the role of mycobactin biosynthesis and transport for growth in 7H9 broth, *M. marinum* wild-type, Δ*mbtB* and Δ*mbtB*-Δ*irtAB*$_{Hyg}$ mutant strains were harvested from stationary phase 7H9 cultures, dispersed by sonication, and inoculated into 7H9 medium. Under these conditions, *M. marinum* wild-type cultures grew robustly over 5 days (OD_{600} ca. 17), whereas both mutant strains did not grow (Figure 3a). As the mutant strains barely grew in minimal medium or on plates used to produce and purify MBT or cMBT, the production of the mycobactins could not be tested. Moreover, since it took the Δ*mbtB*-Δ*irtAB*$_{Hyg}$ double mutant strain as many as ca. 3 weeks to reach only a low density stationary phase, we focused for the following experiments on the Δ*mbtB* mutant strain, which grew considerably faster.

The *M. marinum mbtB* gene is the last gene in a putative operon in the *mbt1* locus (Figure S1), and therefore, the Δ*mbtB* mutant is expected to have no polar effects and should be readily complemented by plasmid-borne *mbtB*. Indeed, Fe-cMBT was isolated by ethyl acetate extraction from supernatants of the genetically complemented Δ*mbtB* mutant strain (Δ*mbtB*/pPK10). The compound yielded a single peak after SEC (A_{450}), identical to Fe-cMBT isolated from wild-type *M. marinum*, and showed the same characteristic red colour with an absorbance maximum at 450 nm (Figure S6a–f). A comparison with the Δ*mbtB* mutant (likely defective for mycobactin production) was not possible, because the strain does not grow in the liquid minimal medium.

Moreover, the *mbtB* gene expressed from P_{tet} on plasmid pFLAG restored growth of the Δ*mbtB* mutant to almost wild-type levels (Figure 3b), whereas introducing *mbtB* expressed from P_{hsp60} on plasmid pMV361 barely increased the growth of the Δ*mbtB* mutant strain (Figure S6g). We did not attempt to express the *mbtB* gene under control of P_{tet} on the pFLAG plasmid in the Δ*mbtB*-Δ*irtAB*$_{Hyg}$ double mutant, because the Δ*irtAB* deletion mutant is apparently not viable unless the *mbtB* is deleted first (see above).

Notoriously, *M. marinum* and other mycobacterial species tend to clump upon growth in broth. Here, we visualised clumping by microscopic analysis of strains producing mCherry, following agarose overlay (Figure 3c). In the course of our experiments, we realised that the Δ*mbtB* and Δ*mbtB*-Δ*irtAB*$_{Hyg}$ mutant strains tend to clump even more extensively than the corresponding *M. marinum* wild-type strain. The "hyper-clumping" phenotype of the Δ*mbtB* strain was reverted by providing the *mbtB* gene expressed from P_{tet} on the pFLAG plasmid (Figure 3c). We also analysed *M. marinum* clumping by flow cytometry (Figure 3d). Compared with wild-type *M. marinum*, "hyper-clumping" of the Δ*mbtB* mutant strain was clearly visible using this approach. However, the addition of purified *M. marinum* MBT or cMBT did not reverse the phenotype. In summary, *M. marinum* Δ*mbtB* and Δ*mbtB*-Δ*irtAB*$_{Hyg}$ are impaired for growth in broth and show a "hyper-clumping" phenotype, which for the Δ*mbtB* mutant strain can be reverted by genetic complementation.

2.5 | Purified Fe-MBT and Fe-cMBT promote the growth of wild type and *mbt* mutant *M. marinum* and *M. smegmatis* in minimal medium

Next, we tested whether purified Fe-MBT and Fe-cMBT affect the growth of *M. marinum* wild-type or mutant strains defective for mycobactin biosynthesis/transport. To this end, the *M. marinum* strains were grown to stationary phase in 7H9 broth, washed with minimal medium, plated onto solidified minimal medium in 24-well plates in the presence or absence of Fe-MBT or Fe-cMBT purified from *M. marinum* or *M. smegmatis*, respectively, and grown for more than 3 weeks (Figure 4a). Under these conditions, the growth of *M. marinum* wild-type and Δ*mbtB* was enhanced by all iron-saturated mycobactins tested, whereas $FeCl_3$ alone had no significant effect (Figure 4a). Quantification by image analysis of the brown-yellow mycobacterial lawns on the minimal medium agar plates revealed that the iron-saturated mycobactins approximately doubled the growth of *M. marinum* wild-type and allowed the growth of the Δ*mbtB* strain, which otherwise did not grow at all (Figure 4b). For all strains tested, Fe-MBT or Fe-cMBT purified from *M. marinum* enhanced the growth of *M. marinum* strains more effectively than Fe-MBT or Fe-cMBT purified from *M. smegmatis*. The growth of the *M. marinum* Δ*mbtB*-Δ*irtAB*$_{Hyg}$ double mutant strain in minimal medium was enhanced by *M. marinum* Fe-cMBT (but not by other mycobactins), suggesting that Fe-cMBT uptake is at least partially independent of the IrtAB transporter. Finally, the addition of purified mycobactins to green fluorescent protein (GFP)-producing *M. marinum* growing in 7H9 medium did not enhance growth (Figure S7) but validated the strong growth phenotype of the Δ*mbtB* or Δ*mbtB*-Δ*irtAB*$_{Hyg}$ mutant strains (Figure 3).

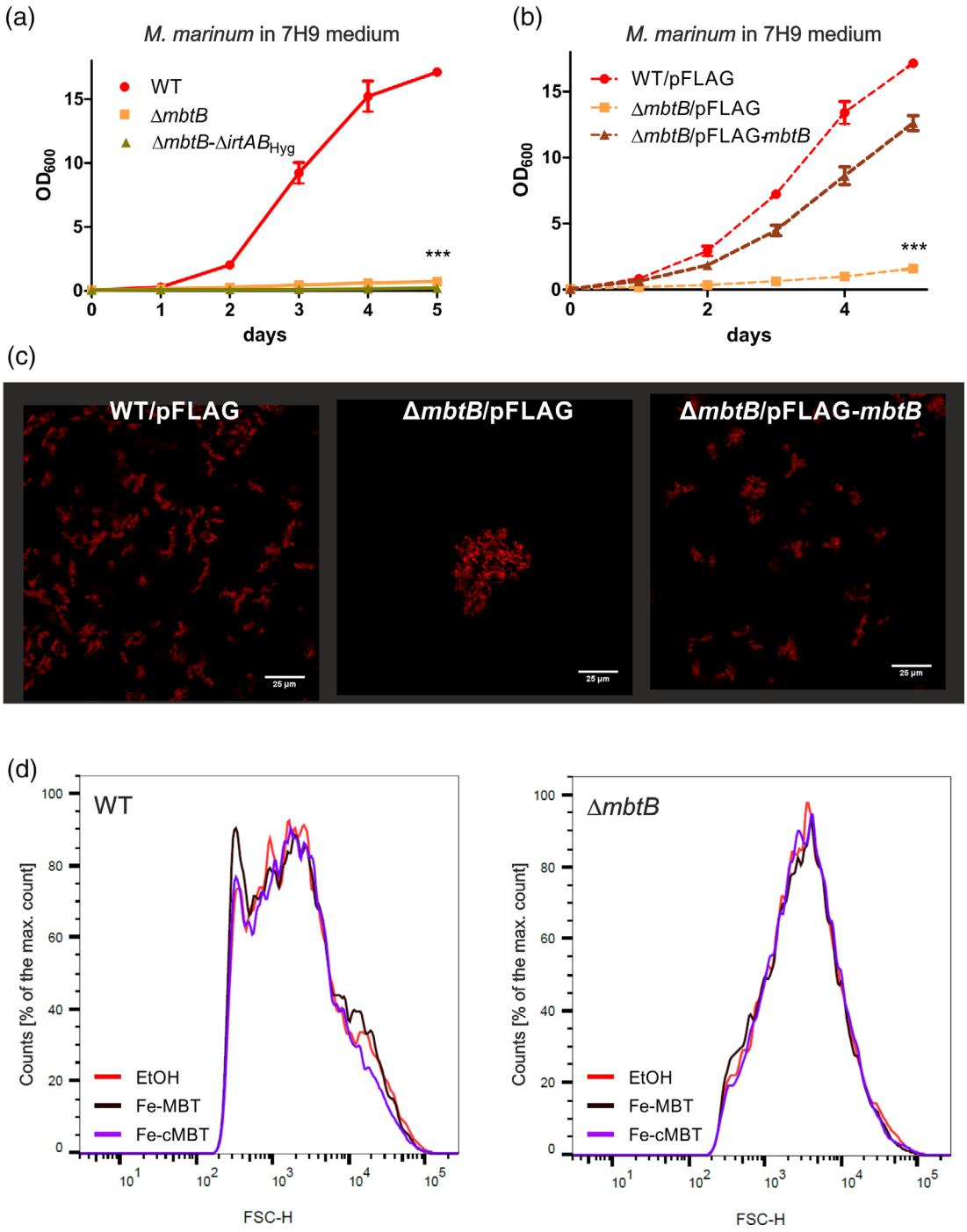

FIGURE 3 *Mycobacterium marinum* Δ*mbtB* and Δ*mbtB*-Δ*irtAB*$_{Hyg}$ are impaired for growth in broth and tend to "hyper-clump." *M. marinum* wild-type, Δ*mbtB* or Δ*mbtB*-Δ*irtAB*$_{Hyg}$ harbouring (a) no plasmid or (b) the vector pHK119 (pFLAG) or pPK10 (pFLAG-*mbtB*) were grown to stationary phase in 7H9 medium, dispersed by sonication, inoculated in 7H9 medium (OD$_{600}$ 0.05), and incubated at 32°C with shaking. At the indicated time points, the OD$_{600}$ of each culture was measured. Data shown represent means and standard deviation of technical triplicates and are representative for two biological replicates (***p < .001; one-way analysis of variance using Dunnett's multiple comparison test; wild type vs. mutant strains, or Δ*mbtB*/pFLAG vs. Δ*mbtB*/pFLAG-*mbtB*). To assess the tendency to clump, (c) mCherry-producing *M. marinum* wild-type or Δ*mbtB* harbouring pCherry10 and pHK119 (pFLAG) or pPK10 (pFLAG-*mbtB*) were grown for 3 days in 7H9 medium, plated into a 24-well plate, covered with liquid agarose, and after solidification, the bacterial clumps were visualised by live-cell imaging, or (d) *M. marinum* wild-type, or Δ*mbtB* harbouring pHK119 (pFLAG) were grown to stationary phase in 7H9 medium, dispersed by sonication, inoculated in 7H9 medium (OD$_{600}$ 0.1) with addition of 10 µM purified *M. marinum* Fe-MBT or Fe-cMBT, or ethanol (control), and incubated at 32°C with shaking. After 3 days, the bacteria were fixed with paraformaldehyde, and the size of bacterial aggregates was analysed by flow cytometry. The graphs show normalised counts of bacterial aggregates as measured by the forward scatter (FSC-H) signal (indicating particle size). Fe-cMBT, ferricarboxymycobactin; Fe-MBT, ferrimycobactin; MBT; mycobactin; WT, wild-type

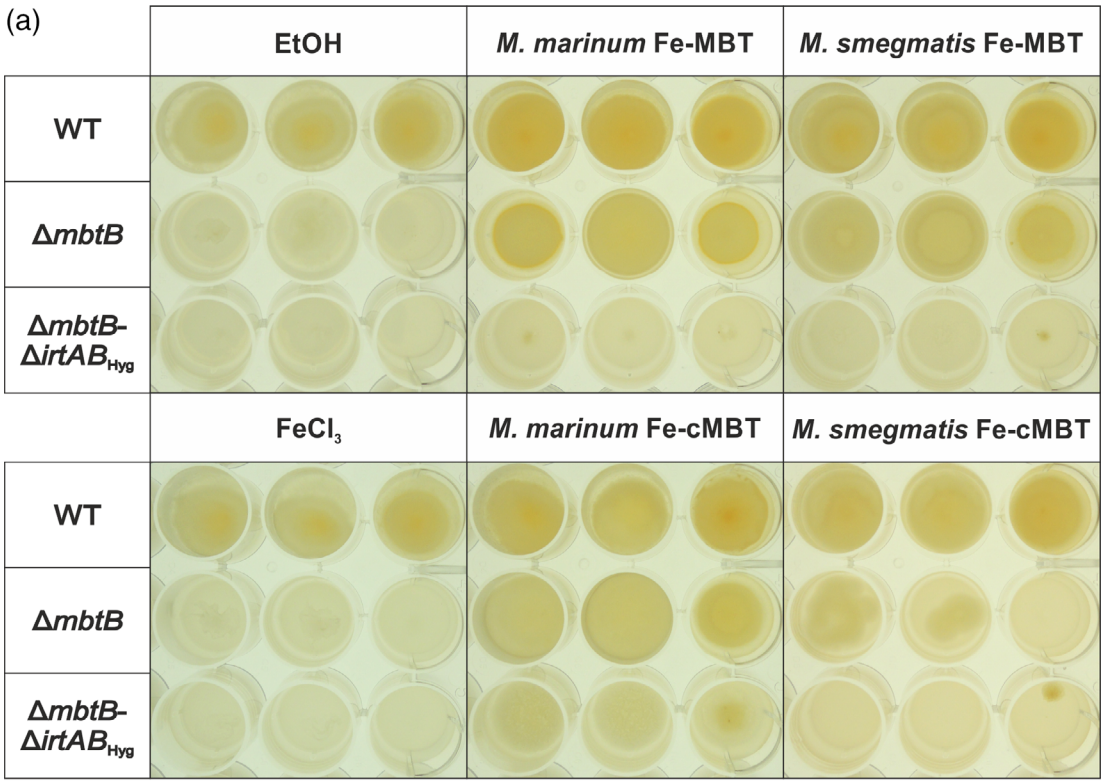

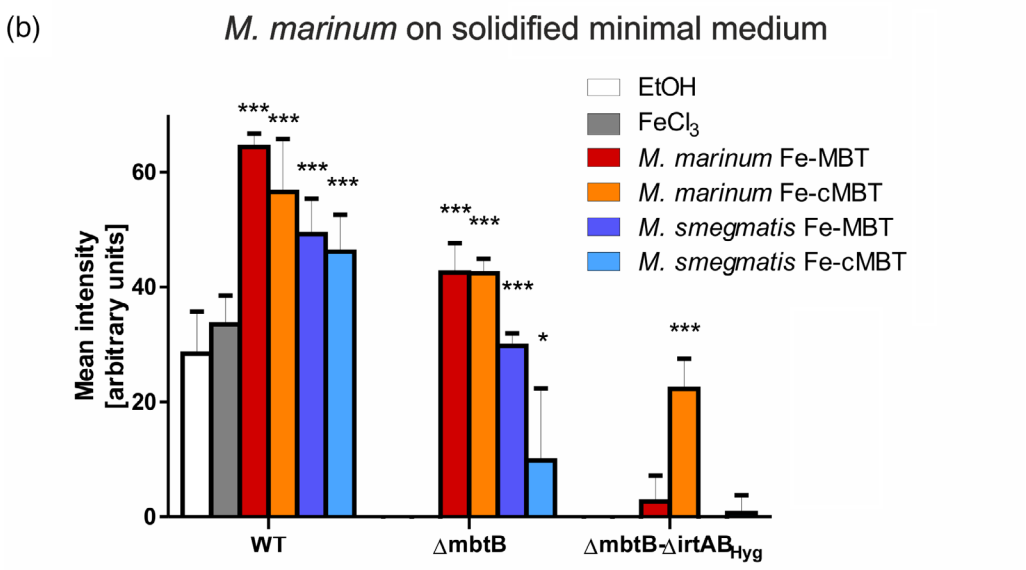

FIGURE 4 Purified Fe-MBT and Fe-cMBT promote the growth of *Mycobacterium marinum* wild-type and Δ*mbtB* on minimal solidified medium. (a) *M. marinum* wild-type, Δ*mbtB*, or Δ*mbtB*-Δ*irtAB*$_{Hyg}$ grown to stationary phase in 7H9 medium were washed with minimal medium, dispersed by sonication, diluted and plated onto solidified minimal medium in 24-well plates (about 2×10^7 CFU per well); 5 μM Fe-MBT or Fe-cMBT from *M. marinum* or *M. smegmatis*, or 5 μM $FeCl_3$ or ethanol (control) were added, and the plates were incubated at 32°C for 3–4 weeks. The images are representative for at least two biological replicates. (b) Bacterial growth was quantified by measuring the mean intensity of the yellow-coloured lawns (a). Data shown represent means and standard deviation of technical triplicates and are representative for two biological replicates (*p < .1, ***p < .001; two-way analysis of variance using Bonferroni's comparison test; control [EtOH] vs. Fe-MBT/Fe-cMBT). Fe-cMBT, ferricarboxymycobactin; Fe-MBT, ferrimycobactin; MBT; mycobactin; WT, wild-type

Taken together, Fe-MBT and Fe-cMBT purified from *M. marinum* or *M. smegmatis* promote the growth of *M. marinum* wild-type and the Δ*mbtB* mutant strain in minimal medium.

We also performed the reciprocal experiments and tested the effects of purified Fe-MBT and Fe-cMBT on the growth in minimal medium of *M. smegmatis*, a fast growing, non-pathogenic

environmental *Mycobacterium* species. To this end, we used *M. smegmatis* wild-type and the mutant strains Δ*fxbA*-Δ*mbtD* (defective for exochelin and mycobactin siderophore biosynthesis) and Δ*fxbA*-Δ*mbtD*-Δ*irtAB* (defective for siderophore biosynthesis and mycobactin transport). To assess the effects of mycobactins on *M. smegmatis*, the wild-type and the mutants were grown to stationary phase in 7H9 broth, diluted (1:100) in minimal medium containing the weak iron chelator 2,2-dipyridyl in 96-well plates in presence or absence of Fe-MBT or Fe-cMBT purified from *M. marinum* or *M. smegmatis*, respectively, and grown for 6 days

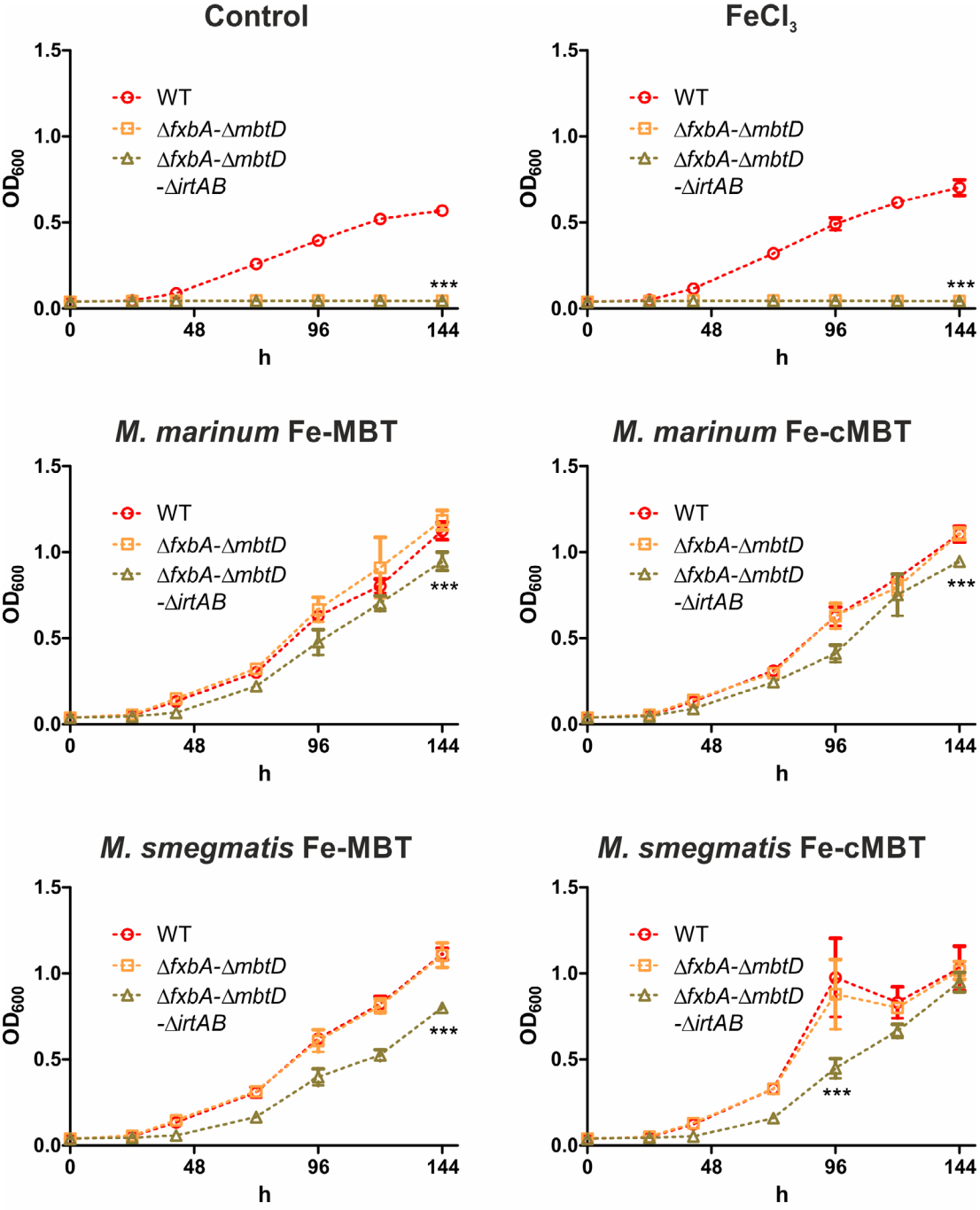

FIGURE 5 Purified Fe-MBT and Fe-cMBT promote the growth of *Mycobacterium smegmatis* wild-type and siderophore mutants in minimal medium. *M. smegmatis* wild-type, Δ*fxbA*-Δ*mbtD*, or Δ*fxbA*-Δ*mbtD*-Δ*irtAB* grown to stationary phase in 7H9 medium were inoculated (1%) in minimal medium, and 10 μM Fe-MBT or Fe-cMBT from *M. marinum* or *M. smegmatis*, or 10 μM $FeCl_3$ or ethanol (control) were added. The cultures were distributed into plastic 96-well plates, incubated at 37°C with shaking (160 rpm), and at the indicated time points, the OD_{600} was measured. Data shown represent means and standard deviation of technical triplicates and are representative for two biological replicates (***$p < .001$; one-way analysis of variance using Dunnett's multiple comparison test; wild type vs. mutant strains). Fe-cMBT, ferricarboxymycobactin; Fe-MBT, ferrimycobactin; MBT; mycobactin; WT, wild-type

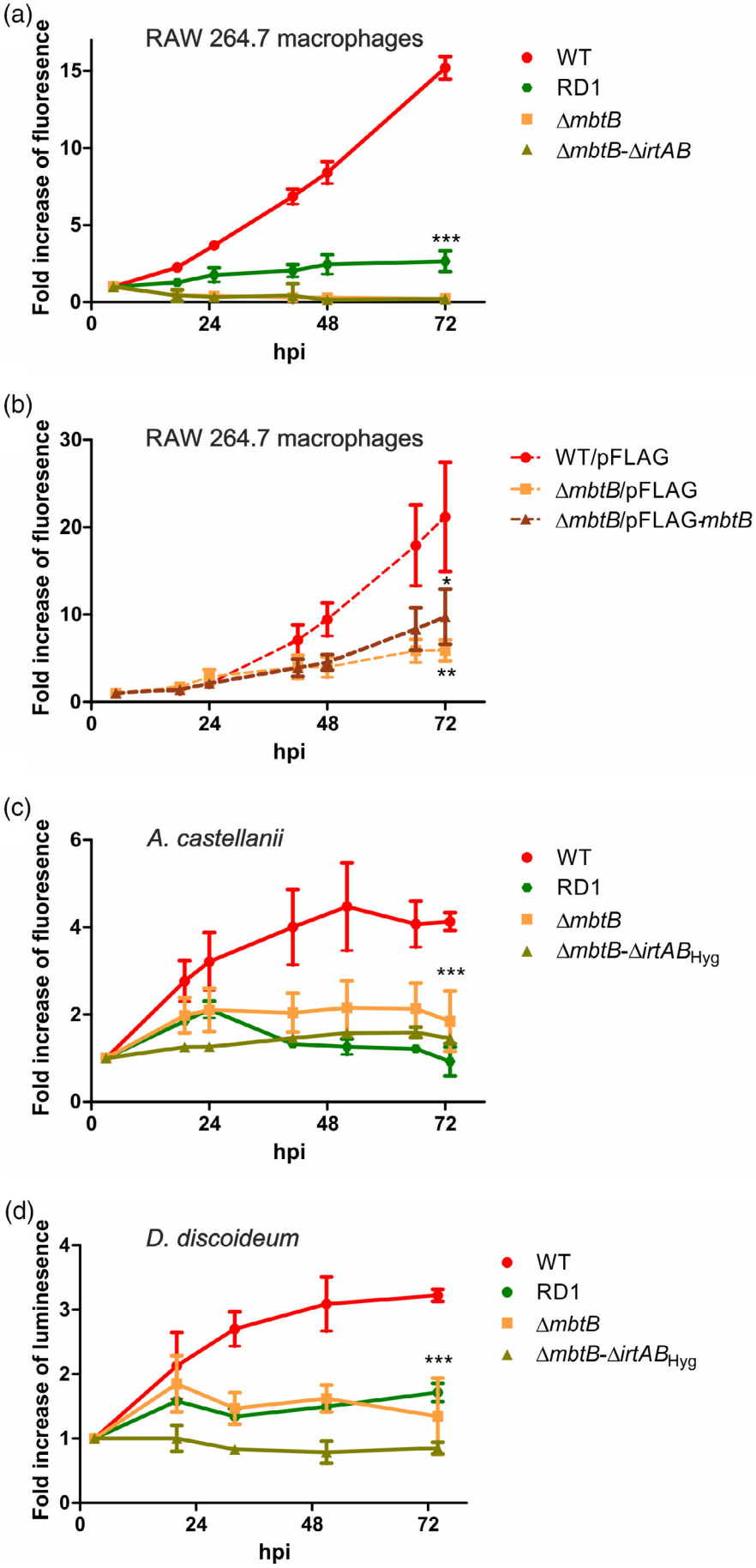

FIGURE 6 *Mycobacterium marinum* Δ*mbtB* and Δ*mbtB*-Δ*irtAB*$_{Hyg}$ are impaired for growth in phagocytes. *M. marinum* wild-type, RD1, Δ*mbtB*, or Δ*mbtB*-Δ*irtAB*$_{Hyg}$ harbouring (a and c) pmsp12::GFP, (b) pcherry10 and pHK119 (pFLAG) or pPK10 (pFLAG-*mbtB*), or (d) pMV306hsp + LuxG13 were grown in 7H9 medium without shaking at 32°C for 4–6 days, dispersed by sonication and spun (500× g, 2 × 10 min) onto (a and b) RAW 264.7 macrophages (MOI 5, 37°C), (c) *A. castellanii* (MOI 20, 25°C), or (d) *D. discoideum* (MOI 5, 25°C) with gentle mixing of the plates and turning them 180° after the first centrifugation to improve bacterial distribution. After 40 min of further incubation, the infected cells were washed several times, detached and seeded into 96-well plates with addition of 5 U ml^{-1} penicillin and 5 μg/ml streptomycin (or 15 μM amikacin; b) to prevent the extracellular growth of bacteria. At the time points indicated (hours postinfection, hpi), bacterial fluorescence or luminescence was recorded with a plate reader. Data shown represent means and standard deviation of technical triplicates and are representative for two biological replicates (*p < .1, **p < .01, ***p < .001; one-way analysis of variance using Dunnett's multiple comparison test; wild-type vs. mutant strains). WT, wild-type

(Figure 5). Under these conditions, the growth of *M. smegmatis* wild-type and Δ*fxbA*-Δ*mbtD* was enhanced by all iron-saturated mycobactins tested compared with the ethanol control, whereas $FeCl_3$ alone allowed only growth of the wild-type strain. Moreover, the addition of siderophores further promoted the growth of wild-type *M. smegmatis* compared with $FeCl_3$, similarly to what was seen for *M. marinum* (Figure 4). Intriguingly, purified *M. marinum* Fe-MBT promoted growth of *M. smegmatis* Δ*fxbA*-Δ*mbtD* as effectively as *M. smegmatis* Fe-MBT. Fe-cMBT purified from *M. marinum* as well as from *M. smegmatis* also enhanced the growth of the Δ*fxbA*-Δ*mbtD*-Δ*irtAB* mutant strain (Figure 5), analogously to *M. marinum* Fe-cMBT stimulating growth of *M. marinum* Δ*mbtB*-Δ$irtAB_{Hyg}$ (Figure 4b), suggesting the existence of other Fe-cMBT uptake system(s) in addition to IrtAB. Taken together, Fe-MBT and Fe-cMBT purified from *M. marinum* or *M. smegmatis* promote the growth in minimal medium of wild-type *M. smegmatis* and siderophore mutant strains, and $FeCl_3$ alone already enhances growth of the wild-type strain.

2.6 | *M. marinum* Δ*mbtB* and Δ*mbtB*-Δ$irtAB_{Hyg}$ are impaired for growth in phagocytes

To assess the contribution of mycobactin production and transport to *M. marinum* virulence and intracellular growth, macrophages or amoebae were infected with fluorescent or luminescent *M. marinum* strains grown in 7H9 medium, and the increase in signal strength was monitored. Fluorescence and luminescence are good proxies for growth of *M. marinum*, because there is a linear relationship between the OD_{600}, CFU, fluorescence, and luminescence (Trofimov et al., 2018). Accordingly, RAW 264.7 macrophages (Figure 6a,b), *A. castellanii* (Figure 6c) or *D. discoideum* (Figure 6d), were infected with fluorescent or luminescent *M. marinum* wild-type, Δ*mbtB*, Δ*mbtB*-Δ$irtAB_{Hyg}$, or the RD1 mutant strain, which lacks the ESX-1 type VII secretion system (T7SS) and is attenuated in host cells (Cosma, Klein, Kim, Beery, & Ramakrishnan, 2006). *M. marinum* wild-type grew robustly in all these phagocytic host cells over the course of 3 days, whereas the Δ*mbtB*, Δ*mbtB*-Δ$irtAB_{Hyg}$, and RD1 mutant strains were severely attenuated and barely grew. For complementation of the Δ*mbtB* mutant strain, the plasmid harbouring *mbtB* under the control of P_{tet} was used (Figure 3b), but intracellular growth in macrophages was only slightly enhanced (Figure 6b). Hence, *M. marinum* strains lacking *mbtB* or *mbtB* and *irtAB* are impaired for growth in phagocytes.

2.7 | Purified *M. marinum* cMBT promotes the intracellular growth of *M. marinum*

Given the inefficient complementation of the intracellular phenotype of the Δ*mbtB* mutant strain, we tested the effects of purified Fe-MBT and Fe-cMBT on intracellular replication of *M. marinum* (Figure 7). In order to avoid potential toxicity for macrophages of bacterial products in the organic extracts of *M. marinum* and *M. smegmatis* mycobactins, Fe-MBT and Fe-cMBT were further purified by SEC. The SEC-purified mycobactins were not toxic for macrophages at concentrations of up to 10 μM, as measured by propidium iodide staining (Figure S8a).

Next, we tested whether externally added mycobactins affect intracellular growth of *M. marinum*. To this end, RAW 264.7 macrophages were infected with GFP-producing *M. marinum* wild-type or Δ*mbtB*, and after uptake and washing away non-internalised bacteria, the infected macrophages were detached and placed into 96-well plates, together with antibiotics preventing extracellular growth and SEC-purified Fe-MBT or Fe-cMBT. Upon exposure of *M. marinum*-infected RAW 264.7 macrophages to 5–10 μM Fe-MBT or Fe-cMBT, only Fe-cMBT from *M. marinum* (but not from *M. smegmatis*) significantly enhanced intracellular growth of wild-type but not of the Δ*mbtB* mutant strain (Figures 7a and S8b,c). Under the same conditions, purified Fe-MBT slightly decreased intracellular growth of wild-type *M. marinum* in macrophages. Upon exposure of *M. marinum*-infected *A. castellanii* to 20 μM Fe-MBT or Fe-cMBT, the mycobactins barely affected intracellular bacterial growth, regardless of whether growth was assessed by fluorescence (Figure 7b) or by luminescence (Figure S9). Alternatively, extracts of Fe-MBT or Fe-cMBT (final concentrations 10 μM) were added to the *M. marinum* cultures in 7H9 medium during bacterial growth. However, using this protocol, neither Fe-MBT nor Fe-cMBT affected the intracellular growth of the wild-type or Δ*mbtB* mutant strain (Figure 7c). Taken together, purified Fe-cMBT enhances intracellular growth of *M. marinum* in macrophages (but not in *A. castellanii*), if added after bacterial uptake but not if only present in *M. marinum* cultures.

2.8 | Coinfection with *M. marinum* wild-type restores the growth defect of Δ*mbtB*

M. marinum lacking *mbtB* showed a stronger growth defect in macrophages compared with amoebae (Figure 6). Yet, despite a more stringent phenotype in macrophages, intracellular growth of *M. marinum* in macrophages but not in *A. castellanii* was promoted by purified Fe-cMBT (Figure 7). Given these results, we used *A. castellanii* to assess whether the Δ*mbtB* mutant strain can be rescued by coinfection with the wild-type strain. To this end, we coinfected amoebae with a luciferase-producing *M. marinum* wild-type or Δ*mbtB* reporter strain together with either wild-type or the Δ*mbtB* mutant strain at a sixfold higher ratio (Figure 8). Under these conditions, the Δ*mbtB* luciferase reporter strain grew intracellularly significantly better upon coinfection with *M. marinum* wild-type compared with coinfection with Δ*mbtB*, at 25°C (Figure 8a) as well as at 30°C (Figure 8b). In fact, if coinfected with the Δ*mbtB* mutant strain, the Δ*mbtB* luciferase reporter strain barely grew, and the wild-type luciferase reporter strain grew less efficiently. In summary, the intracellular growth defect of the Δ*mbtB* mutant strain is restored upon coinfection with the corresponding wild-type but not with the Δ*mbtB* strain.

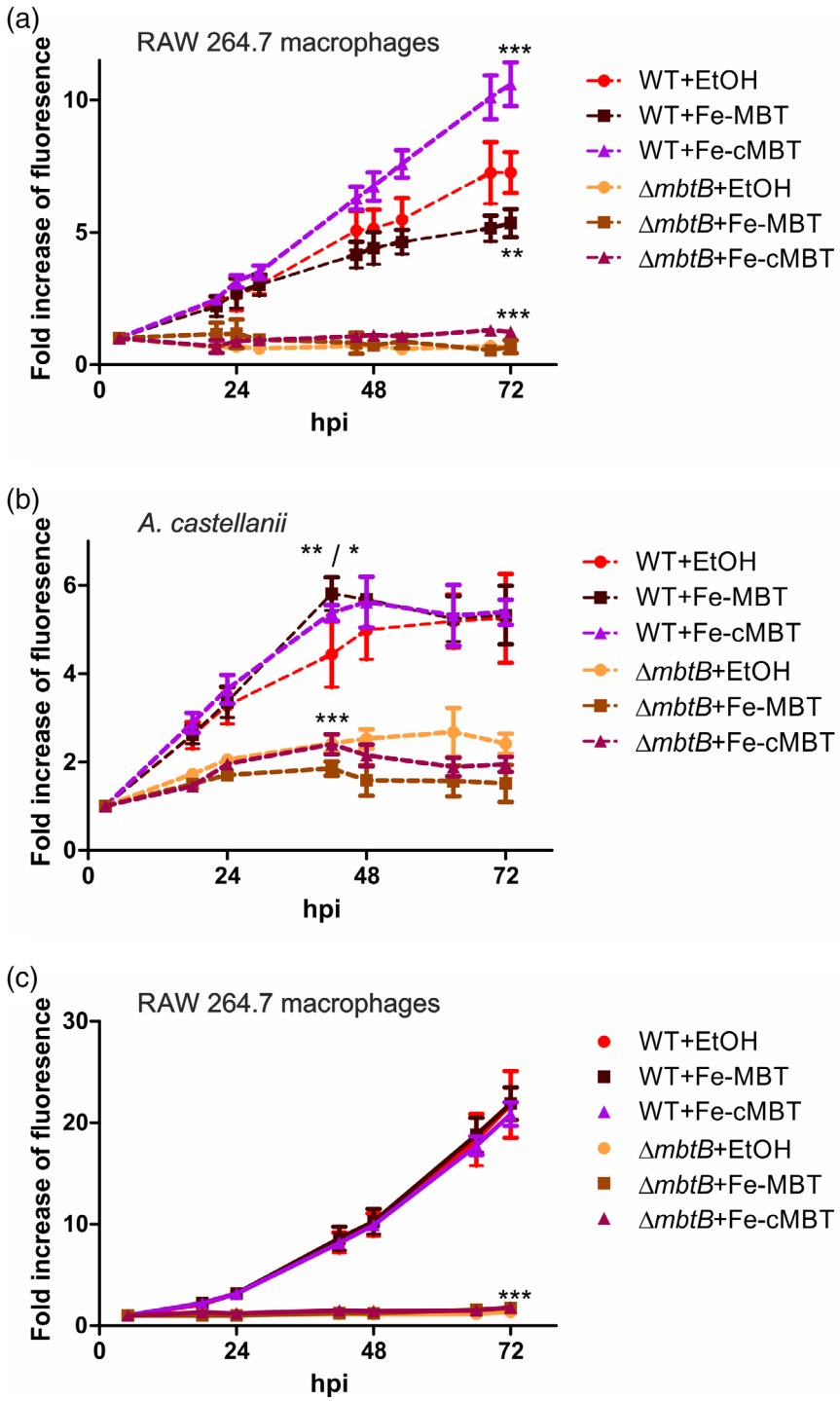

FIGURE 7 Purified *M. marinum* Fe-cMBT promotes the intracellular growth of *Mycobacterium marinum*. (a) RAW 264.7 macrophages or (b) *A. castellanii* amoebae were infected (macrophages: MOI 5, 37°C, 60 min; amoebae: MOI 20, 25°C, 60 min), with stationary phase green fluorescent protein (GFP)-producing *M. marinum* wild-type or Δ*mbtB* (pmsp12::GFP), washed, detached, and seeded into 96-well plates containing minimal medium, and 10 μM (macrophages) or 20 μM (amoebae) SEC-purified *M. marinum* Fe-MBT or Fe-cMBT, or ethanol (control), and 5 U ml^{-1} penicillin as well as 5 μg/ml streptomycin to prevent extracellular bacterial growth. (c) GFP-producing *M. marinum* wild-type or Δ*mbtB* (pmsp12::GFP) was grown in presence of 10 μM *M. marinum* Fe-MBT or Fe-cMBT prior to infection of RAW 264.7 macrophages. Bacterial growth at 30°C was followed with a plate reader using GFP fluorescence as a proxy (a–c). At the time points indicated (hours postinfection, hpi), bacterial fluorescence was recorded with a plate reader. Data shown represent means and standard deviation of technical triplicates and are representative for at least two biological replicates (*p < .1, **p < .01, ***p < .001; one-way analysis of variance using Dunnett's multiple comparison test; wild-type (EtOH) vs. mutant strain or wild-type (EtOH vs. Fe-MBT/Fe-cMBT), respectively). Fe-cMBT, ferricarboxymycobactin; Fe-MBT, ferrimycobactin; MBT; mycobactin; WT, wild-type

3 | DISCUSSION

In this study, *M. marinum* Fe-MBT and Fe-cMBT were purified by organic solvent extraction and identified by MS. The structure of *M. marinum* Fe-cMBT, and in particular the peculiar attachment site of the carboxylated acyl chain, has not been elucidated before. Moreover, a defined *M. marinum* Δ*mbtB* deletion mutant was generated by specialised phage transduction. This strain was defective for extra- and intracellular growth and showed a "hyper-clumping" phenotype. These phenotypes are very similar to observations made with *M. tuberculosis mbt* mutant strains (De Voss et al., 2000; Madigan et al., 2015; Reddy et al., 2013; Tufariello et al., 2016), underscoring the usefulness and accuracy of *M. marinum* as a model organism for pathogenic mycobacteria. The growth defect of the *M. marinum* Δ*mbtB* strain in minimal medium or macrophages was reverted by purified Fe-MBT/Fe-cMBT, or only by Fe-cMBT, respectively. Moreover, the intracellular replication phenotype of Δ*mbtB* in *A. castellanii* was reverted upon coinfection with the wild-type strain, indicating

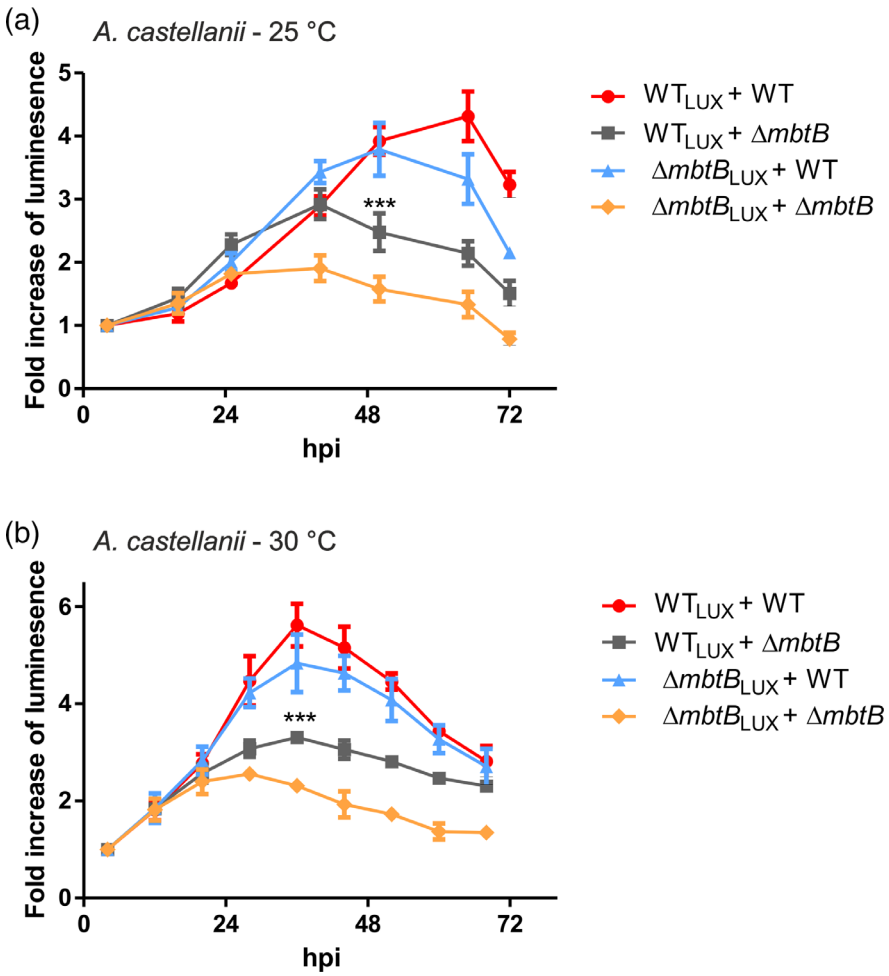

FIGURE 8 Coinfection with *Mycobacterium marinum* wild-type restores the growth defect of Δ*mbtB*. *A. castellanii* were coinfected (60 min) with stationary phase luciferase-producing *M. marinum* wild-type or Δ*mbtB* (MOI = 3) and strains without reporter (MOI = 18), washed, detached, and seeded onto 96-well plates in presence of 5 U mL^{-1} penicillin and 5 μg/mL streptomycin to prevent extracellular growth of bacteria. At the time points indicated (hours postinfection, hpi), bacterial growth at (a) 25°C or (b) 30°C was measured as luciferase activity with a plate reader. Data shown represent means and standard deviation of technical triplicates and are representative for two biological replicates (***$p < .001$; one-way analysis of variance using Dunnett's multiple comparison test; all data compared to wild-type$_{Lux}$/wild-type). WT, wild-type

that the mutant and the parental strain communicate with each other within host cells. Taken together, we showed that *M. marinum* MBT and cMBT play a significant role for extra- and intracellular growth of the pathogen.

M. marinum and other pathogenic or environmental *Mycobacterium* species produce two variants of mycobactin, the hydrophobic MBT and the hydrophilic cMBT. Intriguingly, in *M. marinum* mycobactins, the long acyl side chain (MBT) or the acyl chain with a terminal carboxyl group (cMBT) is attached adjacent to the central ester group of the mycobactin core structure (Figures 1b,e and S3, S4: R_2), whereas in *M. tuberculosis*, *M. smegmatis*, and other mycobacterial species, the long (carboxylated) acyl chain is attached to the peripheral hydroxamate moiety (Chao et al., 2019; Sritharan, 2016). The functional consequences (if any) of these peculiar modifications of *M. marinum* MBT and cMBT are not clear. Perhaps, the overall hydrophobicity of the *M. marinum* mycobactins differs, as compared with mycobactins from other mycobacterial species, allowing a more efficient export/import through the waxy layers of the cell envelope. Despite these substantial structural differences, *M. smegmatis* Fe-MBT and Fe-cMBT reverted the extracellular growth defects of *M. marinum* (Figure 4) and vice versa (Figure 5). Accordingly, the function of a given mycobactin is not confined to a specific mycobacterial species, but rather, mycobactins with different modifications can exert their iron scavenging functions across species barriers.

The sources from which intracellular mycobacteria acquire iron are not well understood. Pathogenic mycobacteria, such as *M. marinum* or *M. tuberculosis*, replicate in host cells in a distinct, membrane-bound pathogen vacuole called MCV, followed by rupture of the vacuole membrane and exit of the bacteria to the cytoplasm (Cardenal-Munoz et al., 2017; Koliwer-Brandl et al., 2019; Russell, 2016). The MCV represents a metal ion-poor environment (Chao et al., 2019), which is depleted of iron due to the activity of NRAMP-1, a proton-driven transporter of ferric iron (Bozzaro, Buracco, & Peracino, 2013; Buracco et al., 2015; Buracco, Peracino, Andreini, Bracco, & Bozzaro, 2017; Peracino, Buracco, & Bozzaro, 2013).

M. marinum strains lacking *mbtB* or *mbtB* and *irtAB* were impaired for intracellular growth already early (24 hpi) during the infection of RAW 264.7 macrophages, *A. castellanii* or *D. discoideum* (Figure 6). At these initial stages of infection, the pathogen still resides in an MCV (Koliwer-Brandl et al., 2019), and therefore, mycobactins likely play a crucial role for scavenging iron in this membrane-bound compartment. Exogenously added mycobactins did not rescue the Δ*mbtB* mutant strain in macrophages or amoebae (Figure 7), presumably reflecting efficient killing in bacteriocidal phagolysosomes of mutant bacteria

defective for mycobactin biosynthesis. Alternatively, the Δ*mbtB* strain is still capable of forming a degradation-resistant MCV, but the exogenously added mycobactins do not reach the compartment. In contrast to Δ*mbtB*, the intracellular growth of wild-type *M. marinum* was enhanced by exogenously added Fe-cMBT. The growth-promoting effect became increasingly apparent at later time points during infection (>48 hpi; Figure 7), and therefore, mycobactin-mediated iron acquisition seems to be particularly important for intracellular growth in the cytoplasm after escape from the MCV. A prominent role for mycobactins at late time points during infection is also supported by the finding that the growth rate of the Δ*mbtB* and Δ*mbtB*-Δ*irtAB*$_{Hyg}$ mutants is much lower compared with wild-type *M. marinum* throughout the infection (Figure 6).

In the iron-depleted environment of the MCV lumen, the secreted cMBT as well as the lipid-bound MBT likely contribute to iron acquisition of *M. marinum*. After escape from the MCV to the host cell cytoplasm, the released cMBT might play a major role in scavenging iron from host sources. However, MBT associated with membranes might also contribute to iron acquisition. Interestingly, MBT (i.e., its gallium complex) was reported to also localise to host cells lipid droplets, which accumulated in the vicinity of phagosomes containing *Escherichia coli* (Luo, Fadeev, & Groves, 2005; McQueen & Groves, 2018). Because mycobacteria utilise lipid droplets to harvest and metabolise lipids (Barisch & Soldati, 2017), it is possible that iron-loaded MBT can be transported to MCVs along this pathway. In general, it is unknown whether and how MBT is released from vesicle or other membranes, or whether the iron bound to MBT is directly utilised by the bacteria.

The release/export pathway of newly synthesised *M. marinum* mycobactins across the bacterial inner membrane is not known. *M. tuberculosis* utilises for this process two transmembrane "mycobacterial membrane protein large" (MmpL) proteins, MmpL4 and MmpL5, along with adaptors of the family of "mycobacterial membrane protein small" (MmpS) proteins, MmpS4 and MmpS5, which associate with the inner membrane on the periplasmic side (Wells et al., 2013; Chalut, 2016; Chao, Sieminski, Owens, & Goulding, 2019). It remains unclear how exactly mycobactins are exported across the periplasm, the cell envelope (cell wall and outer membrane), and the capsule.

The import of iron-loaded mycobactins through the cell envelope and inner membrane is also complex. For *M. tuberculosis*, it has been established that the ESX-3 T7SS secretion system is required for the utilisation of both Fe-MBT and Fe-cMBT. The process likely involves several components of ESX-3; yet, the mechanism underlying this phenomenon remains uncertain (Serafini, Pisu, Palù, Rodriguez, & Manganelli, 2013; Siegrist et al., 2009; Siegrist et al., 2014; Tufariello et al., 2016). The transport of mycobactins across the inner membrane involves the ABC heterodimeric transporter IrtAB, and it has been suggested that Fe-cMBT is the (preferential) substrate (Chao, Sieminski, Owens, & Goulding, 2019; Rodriguez & Smith, 2006; Sritharan, 2016).

IrtA contains a highly conserved, N-terminal siderophore-interacting domain, which likely is involved in reduction of mycobactin-bound ferric to ferrous iron at the cytoplasmic side of the bacterial inner membrane. This facilitates the release of the iron ion from mycobactins and allows recycling of the siderophores (Ryndak et al., 2010). The accumulation of mycobactins must be controlled by the bacteria, as these siderophores become toxic in high doses (Jones et al., 2014). In addition to IrtAB, other transporters and/or reductases might be involved in the transportation of mycobactins across the inner membrane into the cytosol and/or Fe^{3+} reduction (Brown & Ratledge, 1975; Horwitz & Horwitz, 2014; Ratledge, 1971).

Intriguingly, *M. marinum* Fe-cMBT (but not other purified mycobactins) promoted the growth of the *M. marinum* Δ*mbtB*-Δ*irtAB*$_{Hyg}$ mutant strain on minimal medium (Figure 4), and upon exposure of *M. marinum*-infected RAW 264.7 macrophages to purified mycobactins, only Fe-cMBT significantly enhanced intracellular growth of wild-type *M. marinum* (Figures 7a and S8). Together, these findings imply the existence of a Fe-cMBT uptake mechanism independent of the IrtAB transporter and an overall more efficient cell penetration and better bioavailability of Fe-cMBT compared with Fe-MBT. Indeed, cMBT possesses a more amphipathic character, and its hydrophobicity is increased upon binding of iron, because in this state, the hydrophilic hydroxamate and oxazoline groups are engaged with Fe^{3+} and no longer exposed to the aqueous solvent (McQueen & Groves, 2018). Accordingly, Fe-cMBT might also enter the bacterial cytosol by traversing the inner membrane without facilitation by (a) transporter(s). Along the same line, some data support the notion that the carboxylate moiety of cMBT might be esterified (Gobin et al., 1995; Wong, Gobin, Horwitz, & Gibson, 1996; Hodges, Weinberger, Stephens, Horwitz, & Horwitz, 2006; Horwitz et al., 2014), thus also increasing the amphipathic features and membrane permeability of the siderophore.

The *M. marinum* Δ*mbtB* or Δ*mbtB*-Δ*irtAB*$_{Hyg}$ mutant strains were eradicated by RAW 264.7 macrophages and slightly less efficiently also by *A. castellanii* and *D. discoideum* (Figure 6). Yet, in macrophages but not in amoebae, purified Fe-cMBT added postinfection rescued intracellular growth of *M. marinum* wild-type but not the Δ*mbtB* or Δ*mbtB*-Δ*irtAB*$_{Hyg}$ mutant strains (Figure 7a and S9). Interestingly, the intracellular growth of luciferase-producing Δ*mbtB* mutant bacteria improved significantly upon coinfection with the wild-type but not the Δ*mbtB* strain (Figure 8). These findings are in agreement with the notion that the wild-type strain provides the Δ*mbtB* reporter strain with mycobactins, thus fostering its intracellular replication. Additionally, or alternatively, the wild-type strain might provide secreted virulence factors, which support the formation of the replication-permissive MCV or disable the host cell due to toxic effects, thus allowing a more efficient growth of the Δ*mbtB* reporter strain. Wild-type *M. marinum* also promoted the intracellular growth of the luciferase-producing wild-type reporter strain (Figure 8). In contrast, upon addition of (sixfold excess) Δ*mbtB*, the wild-type reporter strain grew less efficiently, in particular at later stages of the infection (>48 hpi). Perhaps, the Δ*mbtB* mutant scavenged mycobactins from the wild-type strain, thereby reducing growth of the latter.

In summary, the biological functions as well as the export and import pathway(s) of mycobacterial mycobactin siderophores are complex and not well understood. In the current study, we document

the prominent role of mycobactins for extra- and intracellular growth of *M. marinum*. The study validates *M. marinum* as a suitable mycobacterial model organism to study mycobactin siderophores and paves the way for a further analysis of their role for extra- and intracellular growth of pathogenic *Mycobacterium* species, including *M. tuberculosis*.

4 | EXPERIMENTAL PROCEDURES

4.1 | Bacterial strains, host cells, and growth conditions

For cloning, *E. coli* strains (Table S5) were grown in LB medium or on LB agar plates at 37°C. If needed, the medium and plates were supplemented with antibiotics: kanamycin (Kan) 50 μg/ml, apramycin (Apr) 10 μg/ml, or hygromycin (Hyg) 100 μg/ml.

M. smegmatis mc^2155 strains (Table S5), unless stated otherwise, were grown at 37°C on 7H10 agar plates supplemented with 10% (v/v) oleic acid/albumin/dextrose/catalase (OADC; Becton Dickinson) and 4% glycerol, or in Middlebrook 7H9 medium supplemented with 10% (v/v) OADC and 0.05% (v/v) Tween 80 (or 0.05% (v/v) tyloxapol (Sigma-Aldrich) for genetics), with shaking (160 rpm). *M. smegmatis* strains were inoculated to broth directly from glycerol stocks.

M. marinum strains (Table S5) were grown at 32°C on 7H10 agar plates supplemented as above, or in 7H9 medium with 10% (v/v) OADC and 0.05% (v/v) tyloxapol, with shaking (150 rpm). If needed, the medium and plates were supplemented with the following antibiotics: Kan 20 μg/ml, Apr 10 μg/ml, or Hyg 50 μg/ml. *M. marinum* strains from glycerol stocks were first plated onto 7H10 agar plates, and colonies were suspended in 7H9 medium for further growth. For infections, *M. marinum* was subcultured from broth into 7H9 medium supplemented additionally with 0.5% (v/v) glycerol and grown for 4 to 6 days without shaking, to reduce bacterial clumping.

A. castellanii (ATCC 30234) was grown at 23°C in PYG medium using proteose peptone (Becton Dickinson) and yeast extract (Difco). *D. discoideum* Ax3 and Ax2 strains were grown axenically at 22–23°C in HL5-C medium containing glucose supplemented with vitamins and microelements (Formedium) and transferred from autoclaved to sterile-filtered medium 1 day prior to infection. RAW 264.7 macrophages were grown in RPMI 1640 medium supplemented with 2 mM L-glutamine and 10% heat-inactivated foetal calf serum (FCS) at 37°C with 5% CO_2. At least 4 days prior to infection, the cells were transferred to Leibovitz L-15 medium (Gibco) supplemented with 10% FCS.

4.2 | Mycobactin production, extraction, and identification

For production of *M. smegmatis* MBT or cMBT, glassware or plasticware, respectively, was used. For *M. marinum* mycobactins, plastic ware was employed throughout. The mycobactins were extracted with organic solvents as detailed below and identified by matrix-assisted laser desorption/ionisation (MALDI)–time of flight (TOF) tandem mass spectrometry (MS/MS) or electrospray ionisation (ESI)-qTOF MS/MS using an Ultraflextreme (Bruker) or Q-Exactive spectrometer (Thermoscientific), respectively.

The minimal medium used to grow *M. smegmatis* or *M. marinum* was adapted from Ratledge et al. (Ratledge & Ewing, 1996): 5 g KH_2PO_4, 5 g L asparagine, 60 ml glycerol in 1 L of H_2O, pH 7.0. The medium was autoclaved with 2% (w/v) Al_2O_3, hot medium was stirred for 15–30 min with suspended Al_2O_3 to remove traces of iron, and filtered with a 0.22 μm filter. The medium was then supplemented with sterile $MgSO_4$ solution (final concentration 1.7 mM) and with $ZnSO_4$ (6.9 μM), $MnSO_4$ (1.8 μM), and $MgSO_4$ (1.6 mM) shortly before addition of bacteria.

For the production of *M. smegmatis* MBT (Snow et al., 1969) and cMBT (Ratledge et al., 1996), stationary phase *M. smegmatis* wild-type strain m^2155 (MBT) or Δ*fxbBC* (cMBT) was grown in 7H9 medium, inoculated 1:1,000 into minimal medium (without additional $FeSO_4$) and grown for another 5–6 days at 37°C with shaking (160 rpm). The Δ*fxbBC* strain (cMBT) was subsequently subcultured 1:100 into fresh minimal medium (containing 0.08 μg/ml $FeSO_4$).

For the production of *M. marinum* MBT, stationary phase cultures grown in 7H9 medium were washed two times and resuspended in minimal medium, spread on agarose minimal medium plates, and grown at 32°C for 4–5 weeks, similarly to protocols published for other mycobacterial species (Hall & Ratledge, 1982; Reddy et al., 2013). To pour plates, 15% (w/v) of agarose NEEO ultra-quality (Roth) was added to basic minimal medium, autoclaved, and supplemented with Zn^{2+}, Mn^{2+}, Mg^{2+}, and Fe^{2+} as outlined above (final concentration 0.32 μg/ml Fe^{2+}). For the production of *M. marinum* cMBT, no iron supplementation was used. *M. marinum* wild-type from stationary phase cultures grown in 7H9 medium was washed two times with minimal medium, resuspended in minimal medium 1:40, and grown for 4–5 weeks at 32°C with shaking (150 rpm). To verify that the genetically complemented Δ*mbtB* mutant strain (see below) produces cMBT, *M. marinum* wild-type or Δ*mbtB* harbouring the plasmid pHK119 (pFLAG) or pPK10 (pFLAG-*mbtB*), respectively, was grown for 8 weeks in liquid minimal medium, and cMBT was extracted as described below.

To obtain MBT, *M. smegmatis* or *M. marinum* cells were collected (by centrifugation of suspensions or scraping from plates, respectively) and suspended in 100% ethanol (ca. 20% of the original culture volume). The cells were stirred overnight at room temperature (RT). The extract was filtered with a 0.22 μm filter and mixed with 1 volume of chloroform. Then 10% (w/v) $FeCl_3$ in 100% ethanol was added dropwise to the solution, until saturation of the red colour was observed. Three fourths of volume of double distilled H_2O was added to form a biphasic solution (chloroform and water/ethanol phases). The organic phase containing Fe-MBT was washed at least twice with 1 volume of H_2O, dried from water leftovers with anhydrous $MgSO_4$, filtered through a filter paper (Whatman), and evaporated. The Fe-MBT extract was then dissolved in 100% ethanol.

For the isolation of cMBT, bacteria were centrifuged, and the supernatant containing the secreted siderophore was filtered with a

0.22 μm filter. The pH was then adjusted to 3.5 with HCl, and 10% (w/v) $FeCl_3$ in 100% ethanol was added dropwise to the solution, until the formation of a precipitate ($FePO_4$) was observed, which after stirring for 1 hr at RT was removed with a 0.22 μm filter. The solution was mixed with 1 volume of ethyl acetate, forming a biphasic solution. The organic phase containing Fe-cMBT was washed at least twice with 1 volume of H_2O, dried with anhydrous $MgSO_4$, filtered through a filter paper (Whatman), and evaporated. The Fe-cMBT extract was then dissolved in 100% ethanol.

For experiments with eukaryotic cells, mycobactins in the extracts were further purified by SEC to remove bacterial products. To this end, the extracts were dried, dissolved in 70% acetonitrile, and injected onto a Superdex Peptide 10/300 GL size-exclusion column (GE Healthcare; 95 μl sample, 50 min run time). The presence of mycobactins was determined by detection of a chromatogram peak at 450 nm. The fractions containing siderophores were collected and evaporated. Dried mycobactins were resuspended in 100% ethanol.

4.3 | Molecular cloning and plasmid construction

The plasmids and primers used in this work are listed in Tables S6 and S7, respectively. Handling of *E. coli* and DNA manipulations were performed according to standard protocols, using kits from Macherey-Nagel. For *M. marinum*, Q5 polymerase (NEB) was used for all PCR amplifications, as this polymerase works with high fidelity at the high GC content (55–65%) of mycobacterial genomic DNA. Calf intestinal alkaline phosphatase (NEB) was used for DNA 5′ and 3′ end dephosphorylation and T4 ligase (NEB) for ligation. The sequences of all PCR products and plasmids generated were confirmed by sequencing.

Isolation of *M. marinum* genomic DNA was done according to Larsen et al. (Larsen, Biermann, Tandberg, Hsu, & Jacobs, 2007). Briefly, bacteria from stationary cultures were centrifuged (10 min, 2,000× g, RT), and the pellet was resuspended with 450 μl GTE solution (4 M guanidine thiocyanate, 0.1 M Tris-Cl, 0.5% sarcosyl), and 50 μl lysozyme solution (10 mg/ml in 25 mM Tris-Cl; Sigma) was added. After overnight incubation, 100 μl 10% sodium dodecyl sulfate (pH 7.2) solution and 50 μl 10 mg/ml proteinase K (Sigma) solution were added and incubated at 55°C for 40 min. After addition of 200 μl 5 M NaCl and 160 μl CTAB (w/v 4.6% NaCl, 11.1% hexadecyltrimethylammonium bromide; Sigma) and further incubation at 65°C for 10 min, the samples were mixed with an equal volume (ca. 1 ml) of chloroform/isoamyl alcohol (v/v 24:1) and centrifuged. The aqueous layer was washed once more with the organic solution and then mixed with isopropanol (0.7× volume). After mixing and short incubation, precipitated DNA was pelleted, washed with 70% alcohol, and resuspended in TE buffer.

To construct complementation plasmids, we used the FX-cloning strategy (Geertsma & Dutzler, 2011) with the backbone pFLAG (Arnold et al., 2018). In this system, the cloned genes are expressed constitutively from the medium strength tetracycline promoter (P_{tet}) and stably integrated into the *attB* site of the genome. The *mbtB* gene was amplified from *M. marinum* DNA in two steps to avoid unspecific PCR products. A 4 kb fragment containing the *mbtB* gene was first amplified using the oPK21/oPK22 primers, followed by using this fragment as a template for the amplification of the *mbtB* gene itself using oPK35/oPK36. The product was cloned into pFLAG creating the complementation plasmid pPK10 and integrated into the genome upon cotransfection with pMA_Int (encoding integrase). The empty pFLAG vector (pHK119) was used as control (Koliwer-Brandl et al., 2019). Initially, we tried to use for genetic complementation the plasmid pMV361-PacI (Koliwer-Brandl et al., 2016), harbouring the *mbtB* gene cloned with the oPK25/oPK26 primers (plasmid pPK9). However, this construct only faintly improved the growth of the Δ*mbtB* mutant strain in 7H9 medium (Figure S5).

4.4 | Transformation of plasmids into mycobacteria

To transform mycobacteria, ca. 1–5 μg of plasmid DNA was electroporated into 400 μl electrocompetent *M. smegmatis* or *M. marinum* using electroporation cuvettes with 0.2 cm electrode gap. A BioRad Gene Pulser was set to 2.5 kV, 1 kΩ, and 25 μF capacitance. Electrocompetent cells were prepared by established protocols (Larsen et al., 2007). In short, a 10 ml bacterial culture was grown to an OD_{600} of 0.8 to 1.0, washed at least twice with 10% glycerol containing 0.05% tyloxapol, and finally concentrated to 1 ml. For *M. smegmatis* or *M. marinum*, the procedure was performed on ice with ice-cold glycerol/tyloxapol or at RT, respectively. After electroporation, 1 ml of 7H9 broth was added for recovery: *M. smegmatis* (2 hr at 37°C without shaking), *M. marinum* (4 hr up to overnight at 32°C) before plating on 7H10 plates containing the desired antibiotics.

4.5 | Generation of defined *Mycobacterium* gene deletion mutant strains

M. marinum deletion mutants were generated as previously described in detail (Koliwer-Brandl et al., 2019). The allelic exchange substrates needed for specialised phage transduction were generated to replace *mbtB* and the two neighbouring genes *irtA* and *irtB* in *M. marinum* with a *γδres-sacB-hyg-γδres* cassette comprising *sacB* and a Hyg resistance gene flanked by the *res* sites of the γδ-resolvase.

The flanking regions of *mbtB* were amplified using the primer pairs oHK13/oHK14 and oHK15/oHK16. Both PCR products were digested with Van91I and ligated with Van91I-digested p0004S vector fragments to obtain the plasmid pHK4. The flanking regions of *irtAB* were amplified using the primer pairs oHK183/oHK184 and oHK185/oHK186. Again, the PCR products were digested with Van91I before ligation with Van91I-digested p0004S vector fragments to obtain the plasmid pHK58.

Both plasmids, pHK4 and pHK58, as well as the DNA of the temperature-sensitive phage phAE159 were linearised with PacI before ligation to obtain pHK18 and pHK60, respectively. High-titre

phages of phAE159Δ*mbtB* and phAE159Δ*irtAB* were prepared in *M. smegmatis* to perform specialised transduction in *M. marinum*, yielding Δ*mbtB*(Hyg). To unmark the Hyg-resistant Δ*mbtB*(Hyg) mutant yielding the strain Δ*mbtB*, the phAE7.1 phage was applied. phAE7.1 harbours the γδ-*tnpR* gene that produces the resolvase to release the *γδres-sacB-hyg-γδres* cassette from a genome. Finally, to construct strain Δ*mbtB*-Δ$irtAB_{Hyg}$, specialised phage transduction using phAE159Δ*irtAB* was performed with the unmarked Δ*mbtB* mutant strain, and double deletion mutants were selected on 7H10/Hyg plates.

The *M. marinum* mutant strains obtained were verified by PCR using primer pairs (Table S7), with one primer located in the genome (*mbtB*-L/-R-ext, *irtAB*-L/-R-ext) and the other primer located in the resistance cassette (oHK33 and oHK36; Figure S5) and sequencing of the amplicon.

M. smegmatis mc^2155 deletion mutants were generated as previously described (Arnold et al., 2018). In brief, upstream and downstream flanking regions of genes of interested were amplified from genomic DNA using primers listed in Table S7, cloned into pINIT, and sequenced, followed by transfer of the flanking regions into pKO (Apr resistance). Electrocompetent *M. smegmatis* was transformed with the pKO vector and plated on 7H10/Apr plates. Apr-resistant clones were tested for the first recombination event by PCR; positive clones were grown in the absence of Apr to allow for a second recombination event and then plated on 7H10 plates containing 20% sucrose and 0.2% 2-deoxygalactose. Clones were screened for deletion of the gene of interest by colony PCR (OneTaq Hot Start DNA Polymerase [M0481]; NEB) and confirmed by PCR from isolated genomic DNA. The following *M. smegmatis* gene deletion mutants (and combinations thereof) were generated in the course of this study: Δ*fxbA* (*msmeg*_0014*)*, Δ*fxbBC* (*msmeg*_0019*)*, Δ*mbtD* (*msmeg*_4512*)*, and Δ*irtAB* (*msmeg*_6553–6554;Table S5). The respective primers to amplify the flanking regions and to verify the gene deletions by PCR are listed in Table S7.

4.6 | RNAseq analysis

D. discoideum infections, RNA extraction, library synthesis, sequencing, and bioinformatics analysis were performed as described by Hanna et al. (https://doi.org/10.1101/590810). Briefly, enrichment of mycobacteria from infected *D. discoideum* cells was carried out by differential lysis of host and mycobacterial cells by guanidine thiocyanate (Chomczynski & Sacchi, 1987). RNA was extracted from cells using the Direct-zol RNA extraction kit (Zymo Research) following the manufacturer's instructions for total RNA isolation with the addition of a mechanical breaking step using a bead beater (FastPrep Instrument). Total RNAs were subjected to cDNA synthesis and NGS library construction using the Ovation Universal System (NuGEN Technologies). rRNAs were depleted by the addition of custom-designed oligonucleotides specific for *D. discoideum* and *M. marinum* rRNAs (5S, 18S, 28S and 5S, 16S, 23S, respectively). Six-plexed samples were pooled in approximately equimolar amounts and run in 50 bp single read flow cells (Illumina, #15022187) on a Hiseq 4000 apparatus (Illumina). 50 nt single-end reads were mapped to the *M. marinum* genome (M strain) using tophat (version 2.0.13) and bowtie2 (version 2.2.4) software. The differential expression analysis was performed using the R package limma, including the data batch effect in the design. The genes showing an adjusted *p*-value lower than .1 and an absolute fold change above 1.5 were considered differentially expressed.

4.7 | Role of mycobactins for mycobacterial growth in minimal medium

M. marinum strains from stationary phase liquid cultures were washed twice with minimal medium (Ratledge & Ewing, 1996), dispersed by sonication, diluted, and plated (about 2×10^7 CFU per well) onto solidified minimal medium in 24-well plates, supplemented with MBT/cMBT, $FeCl_3$ or ethanol (control) as described above. The plates were incubated at 32°C for 3–4 weeks, and pictures of the bacterial lawns were taken and analysed with the FIJI software allowing only to quantify the colours red, green, and blue. In order to quantify the brown-yellow appearance of mycobacterial lawns, the mean intensity of the complementary colour, blue, was measured in the regions of interest (corresponding to the surface of the solidified minimal medium in a well), and the background was subtracted. The values were then multiplied by −1, to account for the blue colour being complementary to yellow, and plotted in the graphs.

M. smegmatis strains were grown in 7H9 medium to stationary phase (4 days) by inoculation from glycerol stocks. These cultures were subcultured 1:100 in 1 ml minimal medium containing 200 μM 2,2-dipyridyl (added from a 1,000× stock in ethanol). Twenty percent Tween 80 stock solutions were autoclaved with 2% (w/v) aluminium oxide and then filtered to remove traces of free iron. The cultures were supplemented with 0.5% (v/v) Tween 80 to avoid cell clumping and supplemented with 10 μM Fe-MBT or Fe-cMBT extracts from *M. marinum* or *M. smegmatis* or 10 μM $FeCl_3$. Cultures were grown at 37°C with shaking (160 rpm) for 6 days in plastic 96-deep well plates (Treff Lab), with each strain grown in triplicates; 50 μl aliquots were taken every 24 hr and transferred to a clear 96-well Microplate (Greiner) for OD_{600} determination with a plate reader.

4.8 | Role of mycobactins for intracellular replication of *M. marinum*

The intracellular growth of *M. marinum* wild-type, Δ*mbtB*, or Δ*mbtB*-Δ$irtAB_{Hyg}$ was determined in *D. discoideum* Ax3 or in *A. castellanii* as described previously (Arafah et al., 2013; Kicka et al., 2014; Koliwer-Brandl et al., 2019), and these protocols were adapted to determine intracellular replication in RAW 264.7 macrophages (Koliwer-Brandl et al., 2019). Briefly, the cells were adapted to the infectious conditions by placing the RAW 264.7 macrophages in Leibovitz/FCS medium for at least 4 days or the *D. discoideum* amoebae in sterile-filtered HL5-C for at least 1 day, respectively. *M. marinum* was

inoculated from stationary phase cultures into fresh standard 7H9 medium, additionally supplemented with 0.5% (v/v) glycerol, and grown under static conditions for 4–6 days. Prior to infections, the bacteria were washed at least once in the appropriate cell culture medium and sonicated three cycles of 80% intensity for 10 s, followed by a 30 s pause (Sonopuls HD2200 with SH-213-G, Bandelin Electronic GmbH & Co. KG, Germany).

M. marinum cultures were then added onto 10 cm dishes of ca. 80% confluent cells at a multiplicity of infection (MOI) of 5 for *D. discoideum* (bacteria producing luciferase), a MOI of 20 for *A. castellanii*, or a MOI of 5 for RAW 264.7 macrophages (bacteria producing GFP). The dishes were centrifuged twice at 500× g for 10 min to increase uptake efficiency. Between the two centrifugation steps, the dishes were turned 180° and gently mixed to avoid accumulation of cells and bacteria on one side of the dish. The dishes were then further incubated for 40 min at 25°C for *D. discoideum* and *A. castellanii* or at 37°C for macrophages before removing extracellular bacteria by intense washes with medium. Finally, the appropriate medium was supplemented with 5 U ml^{-1} penicillin and 5 μg/ml streptomycin (or 15 μM amikacin for mCherry-producing bacteria), conditions which inhibit extracellular but not intracellular growth of *M. marinum* (Barisch, Paschke, Hagedorn, Maniak, & Soldati, 2015).

The infected cells were detached, counted, and seeded in a 96-well plate (black fluorescent or white luminescent plate, Corning). The cell density was adjusted to about 40–50 × 10^3 cells per well and at least one further twofold dilution step. The 96-well plate was sealed with a gas permeable moisture barrier seal (BioConcept). After bacterial uptake and seeding of infected cells, the plates were incubated at 25, 30, or 37°C. A microplate reader (Synergy, BioTek) was used to monitor growth of luminescent or fluorescent *M. marinum* within host cells during the course of infection.

In experiments where purified mycobactins were added after bacterial uptake, the infected cells were seeded into 96-well plates in medium, additionally containing SEC-purified Fe-MBT or Fe-cMBT (final concentration 10 μM) or ethanol (control). For infections with bacteria pre-fed with mycobactins, extracts of Fe-MBT or Fe-cMBT (final concentrations 10 μM), or ethanol as a control, were added to the bacterial 7H9 cultures when inoculated.

In addition to the single strain infections, we also performed coinfections with *A. castellanii* using *M. marinum* strains harbouring a luciferase-producing plasmid or no reporter plasmid; the MOI was 3 and 18, respectively.

4.9 | Confocal microscopy and flow cytometry

For confocal microscopy and flow cytometry, stationary phase mCherry-producing *M. marinum* cultures harbouring pHK119 (FLAG) were dispersed and inoculated in 7H9 medium at an OD_{600} = 0.1. Where indicated, purified *M. marinum* Fe-MBT and Fe-cMBT (10 μM) or ethanol (control) was added. After 3 days of shaking culture (150 rpm, 32°C), bacterial suspensions were plated into 24-well plates and covered with liquid agarose layer (0.05% in phosphate buffered saline). After solidification of the agarose, individual bacteria and bacterial clumps were visualised. Live-cell imaging was performed using a Leica SP8 confocal laser scanning microscope equipped with a 63× 1.4 NA oil immersion objective. Alternatively, after 3 days shaking culture, the bacteria were fixed by addition of paraformaldehyde (final concentration 2%) and analysed by flow cytometry using an LSR II Fortessa (Becton Dickinson) and FlowJo software.

ACKNOWLEDGEMENTS

The plasmids p0004S, phAE159, and phAE7.1 were obtained from William R. Jacobs, Jr (Albert Einstein College of Medicine, Bronx). The plasmids pmsp12::GFP were a gift from Lalita Ramakrishnan (University of Cambridge), pCherry10 was from Tanya Parish (Infectious Disease Research Institute, Seattle), pMV306hsp + LuxG13 from Brian Robertson and Siouxsie Wiles (University of Auckland), and pMV361-PacI was from Rainer Kalscheuer (Heinrich Heine University Düsseldorf). Work in the group of H.H. was funded by the Swiss National Science Foundation (SNF; 31003A_153200, 31003A_175557) and the SystemsX.ch project HostPathX. T.S. received support from multiple grants from the SNF and the SystemsX.ch project HostPathX. Work in the group of M.A.S. was supported by an SNF Professorship (PP00P3_144823), the European Research Council (ERC; consolidator Grant 772190) and a grant of the Foundation for Medical-Biological Research. N. P. received funding from the SNF Ambizione program (PZ00P3_161492), and F.M.A. was supported by a Candoc fellowship of the University of Zurich. Confocal laser scanning microscopy was performed using equipment of the Center of Microscopy and Image Analysis, University of Zurich (UZH). Mass spectrometry and HPLC was performed by Serge Chesnov and Peter Hunziker, respectively, at the Functional Genomics Center of the UZH. The RNAseq bioinformatics analysis was performed by Marco Pagni and Frederic Burdet at the Swiss institute of Bioinformatics (SIB). The funders had no role in study design, data collection and analysis, decision to publish, or preparation of the manuscript.

AUTHOR CONTRIBUTIONS

Conceived and designed experiments: PK, HKB, NH, CB, MAS, TS and HH.

Performed the experiments: PK, HKB, NH, FMA, IG and NP.

Analysed the data: PK, HKB, NH, FMA, IG, NP and CB.

Wrote the paper: PK and HH.

Edited the paper: PK, HKB, NH, FMA, NP, IG, CB, MAS, TS and HH.

Contributed reagents/materials/analysis tools: MAS, TS and HH.

Conflict of Interest: The authors declare no conflict of interest.

ORCID

Hendrik Koliwer-Brandl https://orcid.org/0000-0003-1613-5615
Thierry Soldati https://orcid.org/0000-0002-2056-7931
Hubert Hilbi https://orcid.org/0000-0002-5462-9301

REFERENCES

Arafah, S., Kicka, S., Trofimov, V., Hagedorn, M., Andreu, N., Wiles, S., … Soldati, T. (2013). Setting up and monitoring an infection of *Dictyostelium discoideum* with mycobacteria. *Methods in Molecular Biology*, *983*, 403–417.

Arnold, F. M., Hohl, M., Remm, S., Koliwer-Brandl, H., Adenau, S., Chusri, S., … Seeger, M. A. (2018). A uniform cloning platform for mycobacterial genetics and protein production. *Scientific Reports*, *8*, 9539.

Aubry, A., Mougari, F., Reibel, F. and Cambau, E. (2017). *Mycobacterium marinum*. Microbiol Spectr, *5*.

Barisch, C., Paschke, P., Hagedorn, M., Maniak, M., & Soldati, T. (2015). Lipid droplet dynamics at early stages of *Mycobacterium marinum* infection in *Dictyostelium*. *Cellular Microbiology*, *17*, 1332–1349.

Barisch, C., & Soldati, T. (2017). Breaking fat! How mycobacteria and other intracellular pathogens manipulate host lipid droplets. *Biochimie*, *141*, 54–61.

Barker, L. P., George, K. M., Falkow, S., & Small, P. L. (1997). Differential trafficking of live and dead *Mycobacterium marinum* organisms in macrophages. *Infection and Immunity*, *65*, 1497–1504.

Bouley, D. M., Ghori, N., Mercer, K. L., Falkow, S., & Ramakrishnan, L. (2001). Dynamic nature of host-pathogen interactions in *Mycobacterium marinum* granulomas. *Infection and Immunity*, *69*, 7820–7831.

Bouz, G., & Al Hasawi, N. (2018). The zebrafish model of tuberculosis—No lungs needed. *Critical Reviews in Microbiology*, *44*, 779–792.

Bozzaro, S., Buracco, S., & Peracino, B. (2013). Iron metabolism and resistance to infection by invasive bacteria in the social amoeba *Dictyostelium discoideum*. *Frontiers in Cellular and Infection Microbiology*, *3*, 50.

Brown, K. A., & Ratledge, C. (1975). Iron transport in *Mycobacterium smegmatis*: Ferrimycobactin reductase (NAD[P]H:Ferrimycobactin oxidoreductase), the enzyme releasing iron from its carrier. *FEBS Letters*, *53*, 262–266.

Buracco, S., Peracino, B., Andreini, C., Bracco, E., & Bozzaro, S. (2017). Differential effects of iron, zinc, and copper on *Dictyostelium discoideum* cell growth and resistance to *Legionella pneumophila*. *Frontiers in Cellular and Infection Microbiology*, *7*, 536.

Buracco, S., Peracino, B., Cinquetti, R., Signoretto, E., Vollero, A., Imperiali, F., … Bozzaro, S. (2015). *Dictyostelium* Nramp1, which is structurally and functionally similar to mammalian DMT1 transporter, mediates phagosomal iron efflux. *Journal of Cell Science*, *128*, 3304–3316.

Cardenal-Munoz, E., Barisch, C., Lefrancois, L. H., Lopez-Jimenez, A. T., & Soldati, T. (2017). When Dicty met Myco, a (not so) romantic story about one amoeba and its intracellular pathogen. *Frontiers in Cellular and Infection Microbiology*, *7*, 529.

Chalut, C. (2016). MmpL transporter-mediated export of cell-wall associated lipids and siderophores in mycobacteria. *Tuberculosis*, *100*, 32–45.

Chao, A., Sieminski, P. J., Owens, C. P., & Goulding, C. W. (2019). Iron acquisition in *Mycobacterium tuberculosis*. *Chemical Reviews*, *119*, 1193–1220.

Chomczynski, P., & Sacchi, N. (1987). Single-step method of RNA isolation by acid guanidinium thiocyanate-phenol-chloroform extraction. *Analytical Biochemistry*, *162*, 156–159.

Clark, H. F., & Shepard, C. C. (1963). Effect of environmental temperatures on infection with *Mycobacterium marinum* (Balnei) of mice and a number of poikilothermic species. *Journal of Bacteriology*, *86*, 1057–1069.

Cosma, C. L., Klein, K., Kim, R., Beery, D., & Ramakrishnan, L. (2006). *Mycobacterium marinum* Erp is a virulence determinant required for cell wall integrity and intracellular survival. *Infection and Immunity*, *74*, 3125–3133.

De Voss, J. J., Rutter, K., Schroeder, B. G., Su, H., Zhu, Y., & Barry, C. E., 3rd. (2000). The salicylate-derived mycobactin siderophores of *Mycobacterium tuberculosis* are essential for growth in macrophages. *Proceedings of the National Academy of Sciences of the United States of America*, *97*, 1252–1257.

Geertsma, E. R., & Dutzler, R. (2011). A versatile and efficient high-throughput cloning tool for structural biology. *Biochemistry*, *50*, 3272–3278.

Gobin, J., Moore, C. H., Reeve, J. R., Jr., Wong, D. K., Gibson, B. W., & Horwitz, M. A. (1995). Iron acquisition by *Mycobacterium tuberculosis*: Isolation and characterization of a family of iron-binding exochelins. *Proceedings of the National Academy of Sciences of the United States of America*, *92*, 5189–5193.

Gupta, S., & Rodriguez, G. M. (2018). Mycobacterial extracellular vesicles and host pathogen interactions. *Pathog Dis*, *76*, 76.

Hagedorn, M., Rohde, K. H., Russell, D. G., & Soldati, T. (2009). Infection by tubercular mycobacteria is spread by nonlytic ejection from their amoeba hosts. *Science*, *323*, 1729–1733.

Hagedorn, M., & Soldati, T. (2007). Flotillin and RacH modulate the intracellular immunity of *Dictyostelium* to *Mycobacterium marinum* infection. *Cellular Microbiology*, *9*, 2716–2733.

Hall, R. M., & Ratledge, C. (1982). A simple method for the production of mycobactin, the lipid-soluble siderophore, from mycobacteria. *FEMS Microbiology Letters*, *15*, 133–136.

Harrison, C. F., Kicka, S., Trofimov, V., Berschl, K., Ouertatani-Sakouhi, H., Ackermann, N., … Hilbi, H. (2013). Exploring anti-bacterial compounds against intracellular *Legionella*. *PLoS One*, *8*, e74813.

Hodges, Y. K., Weinberger, H. D., Stephens, J., Horwitz, M. A., & Horwitz, L. D. (2006). Desferri-Exochelin, a lipid-soluble, hexadentate iron chelator, effectively removes tissue iron. *Translational Research*, *148*, 63–71.

Horwitz, L. D., & Horwitz, M. A. (2014). The exochelins of pathogenic mycobacteria: Unique, highly potent, lipid- and water-soluble hexadentate iron chelators with multiple potential therapeutic uses. *Antioxidants & Redox Signaling*, *21*, 2246–2261.

Jones, C. M., Wells, R. M., Madduri, A. V., Renfrow, M. B., Ratledge, C., Moody, D. B., & Niederweis, M. (2014). Self-poisoning of *Mycobacterium tuberculosis* by interrupting siderophore recycling. *Proceedings of the National Academy of Sciences of the United States of America*, *111*, 1945–1950.

Kicka, S., Trofimov, V., Harrison, C., Ouertatani-Sakouhi, H., McKinney, J., Scapozza, L., … Soldati, T. (2014). Establishment and validation of whole-cell based fluorescence assays to identify anti-mycobacterial compounds using the *Acanthamoeba castellanii-Mycobacterium marinum* host-pathogen system. *PLoS One*, *9*, e87834.

Koliwer-Brandl, H., Knobloch, P., Barisch, C., Welin, A., Hanna, N., Soldati, T., & Hilbi, H. (2019). Distinct *Mycobacterium marinum* phosphatases determine pathogen vacuole phosphoinositide pattern, phagosome maturation, and escape to the cytosol. *Cellular Microbiology*, *21*, e13008.

Koliwer-Brandl, H., Syson, K., van de Weerd, R., Chandra, G., Appelmelk, B., Alber, M., … Kalscheuer, R. (2016). Metabolic network for the biosynthesis of intra- and extracellular alpha-glucans required for virulence of *Mycobacterium tuberculosis*. *PLoS Pathogens*, *12*, e1005768.

Larsen, M.H., Biermann, K., Tandberg, S., Hsu, T. and Jacobs, W.R., Jr. (2007).Genetic manipulation of *Mycobacterium tuberculosis*. *Current Protocols in Microbiology*, Chapter 10, *Unit 10A*, 2.

Lienard, J., & Carlsson, F. (2017). Murine *Mycobacterium marinum* infection as a model for tuberculosis. *Methods in Molecular Biology*, 1535, 301–315.

López-Jiménez, A. T., Cardenal-Muñoz, E., Leuba, F., Gerstenmaier, L., Barisch, C., Hagedorn, M., … Soldati, T. (2018). The ESCRT and autophagy machineries cooperate to repair ESX-1-dependent damage at the *Mycobacterium*-containing vacuole but have opposite impact on containing the infection. *PLoS Pathogens*, *14*, e1007501.

Luo, M., Fadeev, E. A., & Groves, J. T. (2005). Mycobactin-mediated iron acquisition within macrophages. *Nature Chemical Biology*, *1*, 149–153.

Madigan, C. A., Martinot, A. J., Wei, J. R., Madduri, A., Cheng, T. Y., Young, D. C., … Moody, D. B. (2015). Lipidomic analysis links mycobactin synthase K to iron uptake and virulence in *M. tuberculosis*. *PLoS Pathogens*, *11*, e1004792.

McMahon, M. D., Rush, J. S., & Thomas, M. G. (2012). Analyses of MbtB, MbtE, and MbtF suggest revisions to the mycobactin biosynthesis pathway in *Mycobacterium tuberculosis*. *Journal of Bacteriology*, *194*, 2809–2818.

McQueen, C. F., & Groves, J. T. (2018). A reevaluation of iron binding by mycobactin J. *Journal of Biological Inorganic Chemistry*, *23*, 995–1007.

Peracino, B., Buracco, S., & Bozzaro, S. (2013). The Nramp (Slc11) proteins regulate development, resistance to pathogenic bacteria and iron homeostasis in *Dictyostelium discoideum*. *Journal of Cell Science*, *126*, 301–311.

Pozos, T. C., & Ramakrishnan, L. (2004). New models for the study of *Mycobacterium*-host interactions. *Current Opinion in Immunology*, *16*, 499–505.

Prados-Rosales, R., Weinrick, B. C., Piqué, D. G., Jacobs, W. R., Casadevall, A., & Rodriguez, G. M. (2014). Role for *Mycobacterium tuberculosis* membrane vesicles in iron acquisition. *Journal of Bacteriology*, *196*, 1250–1256.

Prouty, M. G., Correa, N. E., Barker, L. P., Jagadeeswaran, P., & Klose, K. E. (2003). Zebrafish-*Mycobacterium marinum* model for mycobacterial pathogenesis. *FEMS Microbiology Letters*, *225*, 177–182.

Quadri, L. E., Sello, J., Keating, T. A., Weinreb, P. H., & Walsh, C. T. (1998). Identification of a *Mycobacterium tuberculosis* gene cluster encoding the biosynthetic enzymes for assembly of the virulence-conferring siderophore mycobactin. *Chemistry & Biology*, *5*, 631–645.

Ramakrishnan, L., Federspiel, N. A., & Falkow, S. (2000). Granuloma-specific expression of *Mycobacterium* virulence proteins from the glycine-rich PE-PGRS family. *Science*, *288*, 1436–1439.

Ratledge, C. (1971). Transport of iron by mycobactin in *Mycobacterium smegmatis*. *Biochemical and Biophysical Research Communications*, *45*, 856–862.

Ratledge, C., & Dover, L. G. (2000). Iron metabolism in pathogenic bacteria. *Ann Rev Microbiol*, *54*, 881–941.

Ratledge, C., & Ewing, M. (1996). The occurrence of carboxymycobactin, the siderophore of pathogenic mycobacteria, as a second extracellular siderophore in *Mycobacterium smegmatis*. *Microbiology*, *142*, 2207–2212.

Ratledge, C., Patel, P. V., & Mundy, J. (1982). Iron transport in *Mycobacterium smegmatis*: The location of mycobactin by electron microscopy. *Microbiology*, *128*, 1559–1565.

Reddy, P. V., Puri, R. V., Chauhan, P., Kar, R., Rohilla, A., Khera, A., & Tyagi, A. K. (2013). Disruption of mycobactin biosynthesis leads to attenuation of *Mycobacterium tuberculosis* for growth and virulence. *The Journal of Infectious Diseases*, *208*, 1255–1265.

Rodriguez, G. M., & Smith, I. (2006). Identification of an ABC transporter required for iron acquisition and virulence in *Mycobacterium tuberculosis*. *Journal of Bacteriology*, *188*, 424–430.

Rohde, K. H., Abramovitch, R. B., & Russell, D. G. (2007). *Mycobacterium tuberculosis* invasion of macrophages: Linking bacterial gene expression to environmental cues. *Cell Host & Microbe*, *2*, 352–364.

Rohde, K. H., Veiga, D. F., Caldwell, S., Balazsi, G., & Russell, D. G. (2012). Linking the transcriptional profiles and the physiological states of *Mycobacterium tuberculosis* during an extended intracellular infection. *PLoS Pathogens*, *8*, e1002769.

Russell, D. G. (2016). The ins and outs of the *Mycobacterium tuberculosis*-containing vacuole. *Cellular Microbiology*, *18*, 1065–1069.

Ryndak, M. B., Wang, S., Smith, I., & Rodriguez, G. M. (2010). The *Mycobacterium tuberculosis* high-affinity iron importer, IrtA, contains an FAD-binding domain. *Journal of Bacteriology*, *192*, 861–869.

Schnappinger, D., Ehrt, S., Voskuil, M. I., Liu, Y., Mangan, J. A., Monahan, I. M., … Schoolnik, G. K. (2003). Transcriptional adaptation of *Mycobacterium tuberculosis* within macrophages: insights into the phagosomal environment. *J Exp Med*, *198*, 693–704.

Serafini, A., Pisu, D., Palù, G., Rodriguez, G. M., & Manganelli, R. (2013). The ESX-3 secretion system is necessary for iron and zinc homeostasis in *Mycobacterium tuberculosis*. *PLoS One*, *8*, e78351.

Sharman, G. J., Williams, D. H., Ewing, D. F., & Ratledge, C. (1995). Isolation, purification and structure of exochelin MS, the extracellular siderophore from *Mycobacterium smegmatis*. *The Biochemical Journal*, *305*, 187–196.

Shiloh, M. U., & Champion, P. A. (2010). To catch a killer. What can mycobacterial models teach us about *Mycobacterium tuberculosis* pathogenesis? *Current Opinion in Microbiology*, *13*, 86–92.

Siegrist, M. S., Steigedal, M., Ahmad, R., Mehra, A., Dragset, M. S., Schuster, B. M., … Rubin, E. J. (2014). Mycobacterial Esx-3 requires multiple components for iron acquisition. *MBio*, *5*, e01073–e01014.

Siegrist, M. S., Unnikrishnan, M., McConnell, M. J., Borowsky, M., Cheng, T.-Y., Siddiqi, N., … Rubin, E. J. (2009). Mycobacterial Esx-3 is required for mycobactin-mediated iron acquisition. *Proceedings of the National Academy of Sciences of the United States of America*, *106*, 18792–18797.

Smith, J., Manoranjan, J., Pan, M., Bohsali, A., Xu, J., Liu, J., … Gao, L. Y. (2008). Evidence for pore formation in host cell membranes by ESX-1-secreted ESAT-6 and its role in *Mycobacterium marinum* escape from the vacuole. *Infection and Immunity*, *76*, 5478–5487.

Snow, G. A. (1965). Isolation and structure of mycobactin T, a growth factor from *Mycobacterium tuberculosis*. *The Biochemical Journal*, *97*, 166–175.

Snow, G. A., & White, A. J. (1969). Chemical and biological properties of mycobactins isolated from various mycobacteria. *The Biochemical Journal*, *115*, 1031–1050.

Solomon, J. M., Leung, G. S., & Isberg, R. R. (2003). Intracellular replication of *Mycobacterium marinum* within *Dictyostelium discoideum*: Efficient replication in the absence of host coronin. *Infection and Immunity*, *71*, 3578–3586.

Sritharan, M. (2016). Iron homeostasis in *Mycobacterium tuberculosis*: Mechanistic insights into siderophore-mediated iron uptake. *Journal of Bacteriology*, *198*, 2399–2409.

Tailleux, L., Waddell, S. J., Pelizzola, M., Mortellaro, A., Withers, M., Tanne, A., … Neyrolles, O. (2008). Probing host pathogen cross-talk by transcriptional profiling of both *Mycobacterium tuberculosis* and infected human dendritic cells and macrophages. *PLoS One*, *3*, e1403.

Tobin, D. M., & Ramakrishnan, L. (2008). Comparative pathogenesis of *Mycobacterium marinum* and *Mycobacterium tuberculosis*. *Cellular Microbiology*, *10*, 1027–1039.

Touchette, M. H., & Seeliger, J. C. (2017). Transport of outer membrane lipids in mycobacteria. *Biochimica et Biophysica Acta*, *1862*, 1340–1354.

Trofimov, V., Kicka, S., Mucaria, S., Hanna, N., Ramon-Olayo, F., Del Peral, L. V., … Soldati, T. (2018). Antimycobacterial drug discovery using mycobacteria-infected amoebae identifies anti-infectives and new molecular targets. *Scientific Reports*, *8*, 3939.

Tufariello, J. M., Chapman, J. R., Kerantzas, C. A., Wong, K. W., Vilcheze, C., Jones, C. M., … Jakobs, W. R., Jr. (2016). Separable roles for *Mycobacterium tuberculosis* ESX-3 effectors in iron acquisition and virulence. *Proceedings of the National Academy of Sciences of the United States of America*, *113*, E348–E357.

Tükenmez, H., Edström, I., Ummanni, R., Fick, S. B., Sundin, C., Elofsson, M., & Larsson, C. (2019). *Mycobacterium tuberculosis* virulence inhibitors discovered by *Mycobacterium marinum* high-throughput screening. *Scientific Reports*, *9*, 26.

Wells, R. M., Jones, C. M., Xi, Z., Speer, A., Danilchanka, O., Doornbos, K. S., … Niederweis, M. (2013). Discovery of a siderophore export system essential for virulence of *Mycobacterium tuberculosis*. *PLoS Pathogens*, *9*, e1003120.

White, A. J., & Snow, G. A. (1968). Methods for the separation and identification of mycobactins from various species of mycobacteria. *The Biochemical Journal*, *108*, 593–597.

Wilson, B. R., Bogdan, A. R., Miyazawa, M., Hashimoto, K., & Tsuji, Y. (2016). Siderophores in iron metabolism: From mechanism to therapy potential. *Trends in Molecular Medicine*, *22*, 1077–1090.

Wong, D. K., Gobin, J., Horwitz, M. A., & Gibson, B. W. (1996). Characterization of exochelins of *Mycobacterium avium*: Evidence for saturated and unsaturated and for acid and ester forms. *Journal of Bacteriology*, *178*, 6394–6398.

World Health Organization. (2019). *Global tuberculosis report 2019*. https://www.who.int/tb/publications/global_report/en/.

SUPPORTING INFORMATION

Additional supporting information may be found online in the Supporting Information section at the end of this article.

How to cite this article: Knobloch P, Koliwer-Brandl H, Arnold FM, et al. *Mycobacterium marinum* produces distinct mycobactin and carboxymycobactin siderophores to promote growth in broth and phagocytes. *Cellular Microbiology*. 2020; 22:e13163. https://doi.org/10.1111/cmi.13163